Desalination 550 (2023) 116370

Contents lists available at ScienceDirect

Desalination

journal homepage: www.elsevier.com/locate/desal

Correlating the role of nanofillers with active layer properties and performance of thin-film nanocomposite membranes

Lamar A. Perry [a,b], Nick Guan Pin Chew [a], Kasia Grzebyk [a], Pinar Cay-Durgun [c], Mary Laura Lind [c], Paban Sitaula [d], Mustapha Soukri [d], Orlando Coronell [a,*]

[a] Department of Environmental Sciences and Engineering, Gillings School of Global Public Health, The University of North Carolina at Chapel Hill, Chapel Hill, NC 27599-7431, USA
[b] Curriculum in Applied Sciences and Engineering, The University of North Carolina at Chapel Hill, Chapel Hill, NC 27599-7431, USA
[c] School for Engineering of Matter, Transport, and Energy, Arizona State University, Tempe, AZ 85287, USA
[d] RTI International, 3040 East Cornwallis Road, Research Triangle Park, Durham, NC 27709-2194, USA

HIGHLIGHTS

- Nanofillers were embedded into TFN active layers at <1 at.%.
- Physico-chemical characterizations of active layers were representative of polymer.
- Salt rejection above nanofiller loading threshold of ~0.15 wt% was markedly lower.
- Changes in membrane physico-chemical properties and performance were not correlated.
- Flow through nanofiller/along nanofiller-polymer interface likely boosts permeance.

GRAPHICAL ABSTRACT

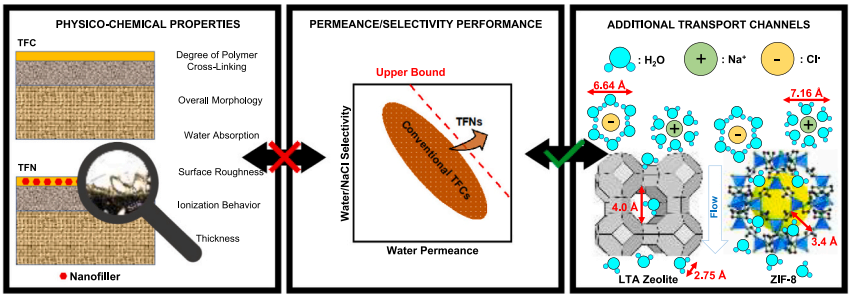

ARTICLE INFO

Keywords:
Thin-film nanocomposite
Polyamide
Zeolite
Zeolitic imidazolate framework
Membrane
ZIF-8

ABSTRACT

Thin-film nanocomposite (TFN) membranes are emerging water-purification membranes that could provide enhanced water permeance with similar solute removal over traditional thin-film composite (TFC) membranes. However, the effects of nanofiller incorporation on active layer physico-chemical properties have not been comprehensively studied. Accordingly, we aimed to understand the correlation between nanofillers, active layer physico-chemical properties, and membrane performance by investigating whether observed performance differences between TFN and control TFC membranes correlated with observed differences in physico-chemical properties. The effects of nanofiller loading, surface area, and size on membrane performance, along with active layer physico-chemical properties, were characterized in TFN membranes incorporated with Linde Type A (LTA) zeolite and zeolitic imidazole framework-8 (ZIF-8). Results show that nanofiller incorporation up to ~0.15 wt% resulted in higher water permeance and unchanged salt rejection, above which salt rejection decreased 0.9–25.6 % and 26.1–48.3 % for LTA-TFN and ZIF-8-TFN membranes, respectively. Observed changes in active layer physico-chemical properties were generally unsubstantial and did not explain observed changes in TFN

* Corresponding author.
E-mail address: coronell@unc.edu (O. Coronell).

https://doi.org/10.1016/j.desal.2023.116370
Received 2 October 2022; Received in revised form 2 January 2023; Accepted 2 January 2023
Available online 19 January 2023

membrane performance. Therefore, increased water permeance in TFN membranes could be due to preferential water transport through porous structures of nanofillers or along polymer-nanofiller interfaces. These findings offer new insights into the development of high-performance TFN membranes for water/ion separations.

1. Introduction

Membranes used in reverse-osmosis (RO) and nanofiltration (NF) applications typically consist of three chemically distinct layers arranged in a thin-film composite (TFC) configuration—a top ultra-thin polyamide-based active layer (~20–200 nm) synthesized *via* interfacial polymerization on an intermediate microporous polysulfone support (~20–50 μm), backed by a porous, non-woven polyester backing (~50–150 μm) [1–4]. TFC membranes are commonly used in the production of clean water from saline and other impaired water sources to remove a suite of contaminants of concern [2,5,6]. Researchers have steadily improved TFC membrane performance through the modification of physico-chemical properties or molecular structures of the active layer [7–28], but water/ion separation performance has been curtailed by the permselectivity trade-off [29–32].

Drawing inspiration from polymeric membranes modified with inorganic nanomaterials as a means to enhance permselectivity for gaseous separations [33], scientists have incorporated nanoparticles (*i.e.,* nanofillers) into active layers of membranes termed thin-film nanocomposite (TFN) membranes for water remediation and desalination [1,4,10,11,34–39]. Jeong et al. used single-crystal Linde Type A (LTA) nano-zeolites as nanofillers in water-purification membranes [10]. Nano-zeolites have large pore volumes, cage-like frameworks, narrow-size pore distributions, and hydrophilic surfaces [10,35,40–44]. Results show that TFN membranes prepared with porous zeolite nanofillers had higher water permeances than with non-porous nanofillers, but water permeance for both types of TFN membranes were enhanced without negative impacts on salt-rejection performances; the expected permselectivity trade-off was not observed. Since then, a plethora of studies have reported on the effects of mobile cations (*e.g.,* sodium, Na^+ and silver, Ag^+) [35], zeolite crystal size [40], and post-treatment regimens on membrane water permeance and/or contaminant rejection [41], including comparisons between the performance of commercially available TFN membranes and that of existing commercially available RO products [42–44].

Other potential nanofillers for water-purification applications include silica [45–49], graphene oxide [50–54], carbon nanotube [55–63], titania [64–66], and metal-organic frameworks (MOFs) [67–82]. Among them, MOFs are promising for water-purification applications [83–85] ascribing to their tunable physico-chemical properties and multiple functionalities [86–89], but only few classes of MOF materials possess the required physico-chemical stability, robustness, and hydrolytic stability [86,87,90]. Zeolitic imidazole framework (ZIF) is an example of a suitable MOF for water-purification applications [91–97]. ZIFs are topologically isomorphic with zeolites, but ZIFs possess ~2–4 times as much surface area and pore volume and, more importantly, the tunable features that zeolites lack [98,99]. Specifically, ZIF-8 nanoparticles have pore diameters and apertures of 11.6 and 3.4 Å, respectively [86,87], rendering them potential alternatives to LTA zeolites (11.05 and 4.21 Å, respectively [10,100–103]). Theoretically, the pore apertures in ZIF-8 are large enough to allow for water passage (2.75 Å) while remaining impermeable to hydrated ions such as Na^+ (7.16 Å) and chloride (Cl^-, 6.64 Å) [67,69,104,105]. Several studies have previously investigated the use of ZIF-8 nanofillers in membrane filtration [69,70,77–80,82,106–108].

Numerous works have attempted to elucidate the mechanism(s) behind TFN membranes' superior water- and ion-transport properties, but proposed mechanisms remain debatable and controversial [41,67,101,109–114]. Using molecular dynamic simulation, Turgman-Cohen et al. discovered that dense, highly structured water regions at the polymer-nanofiller interface in TFN membranes formed barriers to water transport, bringing about lower water permeance [101]. Additionally, a water depletion layer was formed near the surface of hydrophobic nano-zeolites, further impeding water transport. In another study, results suggest that water flow at the polymer-nanofiller interface was slightly higher than that through the nanofillers (*i.e.,* 17.3 % higher) [114]. Based on experimental evidence and Raman microscopic mapping analysis, Lee et al. inferred that porous nanofillers provide water-permeable channels in TFN membranes [67]. Yin et al. [113] found that TFN membranes embedded with hydrophilic non-porous nanofillers exhibited enhanced water permeance (*i.e.,* 26.9 %) while maintaining salt selectivity due to the formation of nanochannels at polymer-nanofiller interfaces [115]. These highly permeable water channels at the polymer-nanofiller interface were non-existent in TFN membranes incorporated with hydrophobic non-porous nanofillers [113], which was in good agreement with previous literature [116,117]. In the same Yin et al. study, the addition of hydrophobic and hydrophilic porous nanofillers resulted in permeance enhancement of 18.3 % and 51.9 %, respectively. In the case of hydrophobic porous nanofillers, water flows preferentially through nanochannels present within their porous structures. On the other hand, the synergistic effects of exterior (*i.e.,* polymer-nanofiller interface) and interior (*i.e.,* nanofiller pores) nanochannels in TFN membranes embedded with hydrophilic porous nanofillers brought about improved interconnectivity among these channels, resulting in permeance enhancement greater than the sum of their individual contributions. Overdosing nanofillers could form aggregates and result in negligible enhancement in water permeance in TFN membranes [39,118].

Thus far, no study has systematically evaluated the effects that nanofillers have on the physico-chemical properties of polyamide active layers or how those effects correlate to changes in membrane performance [119,120]. Accordingly, the overall goal of this study was to advance the understanding of the correlation between nanofillers, physico-chemical properties, and performance. Specifically, the objectives were to (i) investigate the effects of nanofiller loading, surface area, and size on the physico-chemical properties of TFN membrane active layers containing either LTA nano-zeolites or ZIF-8 as nanofillers [121]; and (ii) evaluate whether the observed effects on physico-chemical properties correlate with observed changes in membrane performance in terms of water permeance and NaCl rejection. All membranes had polyamide-based active layers similar to those of commercial TFC membranes. The active layer physico-chemical properties characterized consisted of properties known to impact membrane performance, including degree of polymer cross-linking [122], ionization behavior [123], water absorption [124], thickness [125], surface roughness [126], and cross-sectional morphology [127]. This work is expected to contribute to advancing the fundamental understanding of the mechanisms by which nanofillers affect membrane performance.

2. Materials and methods

2.1. Chemicals and solvents

A.C.S. certified cesium chloride (CsCl, 99.999 %), cesium hydroxide monohydrate (CsOH, 99.95 %), zinc nitrate hexahydrate ($Zn(NO_3)_2{\cdot}6H_2O$, ≥99 %), silver nitrate ($AgNO_3$, ≥99 %), *m*-phenylenediamine (MPD, 99 %), and *n*-hexane (anhydrous, 95 %) were obtained from Sigma-Aldrich® (Saint Louis, MO). A.C.S. certified *N*,*N*-dimethylformamide (DMF), nitric acid (HNO_3, 70 %), hydrochloric acid (HCl, 37 %), sodium hydroxide (NaOH), sodium chloride (NaCl, ≥99 %),

ethanol (95 %), methanol (≥99.8 %), hydrogen peroxide (H_2O_2, 30 % in water), ammonium hydroxide (NH_4OH, 25 %), and 2-methylimidazole (98 %) were acquired from Fisher Scientific (Pittsburgh, PA). Trimesoyl chloride (TMC) and Isopar™ G fluid were purchased from Spectrum Chemicals (New Brunswick, NJ) and Univar (Raleigh, NC), respectively. All chemicals and solvents were used as received without further purification.

2.2. Nano-zeolites

LTA nano-zeolites (4A, Na^+) were used as nanofillers in the fabricated TFN membranes. The LTA nano-zeolites were obtained from NanoScape AG (Planegg, Germany). The zeolite nanofillers had sizes of ~100 nm in diameter according to the manufacturer specifications [128].

2.3. Synthesis of ZIF-8 nanofillers

All ZIF-8 materials were prepared in the laboratory using modified procedures adopted from multiple sources [70,98,99]. $Zn(NO_3)_2{\cdot}6H_2O$ (4.4 g) was added to 24 g of methanol. 2-methylimidazole (9.8 g) was added to 240 g of methanol. The $Zn(NO_3)_2{\cdot}6H_2O$ solution was added to the 2-methylimidazole solution over a period of ~4 s, stirred at 1000 rpm for 5 min, then allowed to sit undisturbed for two days. The resulting colloidal mixture was centrifuged for purity, rinsed with laboratory-grade water (resistivity: ≥17.8 MΩ.cm and total organic carbon: <0.2 mg C/L) from a Dracor ultrapure-water system (Durham, NC), transferred to an open glass dish, covered with a large Kimwipe, and allowed to sit in air for at least 3 h. Subsequently, the glass dish was covered with foil, placed in a -4 °C freezer for 6 h, then freeze dried. The resulting ZIF-8 nanofillers had a diameter and surface area of ~100 nm and 1148.41 ± 8.29 m^2/g, respectively (see Fig. A.2(a) and (b) and Table A.2). The ZIF-8 product yield averaged ~40 % based upon the formula $C_8H_{10}N_4Zn$.

Additional batches of ZIF-8 nanofillers were prepared with different surface areas and particle sizes (Fig. A.2(c)–(f)). To prepare ZIF-8 nanofillers with different surface areas, the ZIF-8 nanofillers prepared as described above were calcined at temperatures of 350, 450, or 550 °C for 1 h, and then at 1000 °C for 8 h before being allowed to cool under a nitrogen purge (see detailed protocol in Section A1 in the Appendix). The calcination procedure involving the heating steps at 350, 450, and 550 °C resulted in Brunauer–Emmett–Teller (BET) surface areas of 301.99 ± 20.27, 268.55 ± 17.52, and 0.96 ± 0.48 m^2/g, respectively. To prepare ZIF-8 nanofillers with different diameters, ZIF-8 nanofillers were produced as described above, but with one of the following changes in the experimental procedure: (i) addition of the Zn $(NO_3)_2{\cdot}6H_2O$ solution into the 2-methylimidazole solution at a rate of ~3 mL/min (instead of over ~4 s) which resulted in ZIF-8 nanofillers with a diameter of ~150 nm and BET surface area of 747.58 ± 9.87 m^2/g; (ii) doubled the methanol solvent volumes to 48 g for the Zn $(NO_3)_2{\cdot}6H_2O$ solution and 480 g for the 2-methylimidazole solution (instead of 24 g and 240 g, respectively), which resulted in ZIF-8 nanofillers with a diameter of ~30 nm and BET surface area of 795.97 ± 16.53 m^2/g; (iii) no stirring after the addition of the $Zn(NO_3)_2{\cdot}6H_2O$ solution to the 2-methylimidazole solution (instead of mixing for 5 min), which resulted in ZIF-8 nanofillers with a diameter in the 20–200 nm range and BET surface area of 1275.27 ± 20.48 m^2/g; and (iv) stirring time of 15 s (instead of 5 min), which resulted in ZIF-8 nanofillers with a diameter of ~65 nm and BET surface area of 1322.20 ± 19.85 m^2/g. Hereon, these four modified procedures will be referred to as (i) titration; (ii) double solvent; (iii) no stirring; and (iv) 15-s stirring. Note that it was not possible to vary only the ZIF-8 nanofiller size, but rather changes in size were accompanied by changes in BET surface area. Representative electron microscopy images of ZIF-8 nanofillers fabricated in this study can be found in Figs. A.1(a)–(c) and A.2(a)–(f) in the Appendix. X-ray diffraction (XRD) patterns of all samples are provided in Fig. A.3.

2.4. Membrane supports

Pre-cast PS20 polysulfone membrane supports were provided by Nanostone Water (Eden Prairie, MN). Prior to use, all PS20 support sheets (18 × 18 cm^2) were sprayed with ethanol, thoroughly rinsed with laboratory-grade water, and stored for 48 h at room temperature in a 1-L Nalgene bottle filled with fresh laboratory-grade water.

2.5. Incorporation of nanofillers into active layers during polyamide casting

Control TFC membranes were hand-cast *via* the interfacial polymerization process (*i.e.,* 1 min of reaction time) between MPD (3.5 wt% in laboratory-grade water) and TMC (0.15 wt% in Isopar™ G) on preformed PS20 polysulfone supports as described in our previous works [13–16,129] and elsewhere in the literature [3,35,130–132]. For the nano-zeolite study, TFN membranes were prepared with LTA nano-zeolite loadings of 0.015, 0.15, 0.30, and 0.75 wt% in TMC solutions. Hereon, TFN membranes containing LTA nano-zeolites will be referred to as LTA-TFNs. As part of the ZIF-8 study, TFN membranes were prepared using TMC solutions containing ZIF-8 nanofillers (~100 nm in diameter) at loadings of 0.015, 0.15, 0.30, and 0.75 wt%. TFN membranes containing ZIF-8 nanofillers will be known as ZIF-8-TFNs from here on out. To study the effects of ZIF-8 surface area on membrane performance, TFN membranes were prepared with carbonized ZIF-8 nanofillers (0.15 wt% in TMC solutions) having BET surface areas of 301.99 ± 20.27, 268.55 ± 17.52, and 0.96 ± 0.48 m^2/g (see Section 2.3). To evaluate the effects of ZIF-8 size on membrane performance, ZIF-8-TFNs were cast with TMC solutions containing ZIF-8 nanofillers (0.15 wt% in TMC solutions) having diameters of ~30, ~65, ~150, and ~20–200 nm. Additional information on the fabrication procedures of the respective TFC and TFN membranes can be found in Section A4.

2.6. Membrane physico-chemical characterizations

For physico-chemical characterizations, membrane coupons with a size of 2.5 × 5.0 cm^2 were cut from the membrane sheets (18 × 18 cm^2). Active layer physico-chemical properties such as elemental composition, concentration of charged sites, ionization behavior, degree of polymer cross-linking, water absorption, thickness, surface roughness, and overall morphology were characterized using methods previously established in the literature [122,123,125,127,133–136]. In the ZIF-8 study, we focused the characterization work on the group of ZIF-8-TFNs used to study the effects of ZIF-8 loading on membrane performance (Section 3.1.1) because these membranes showed significantly different performances from one another in terms of both water permeance and NaCl rejection. Given that the group of ZIF-8-TFNs used to study the effects of ZIF-8 size on membrane performance (Section 3.1.2) showed significantly different performances from one another only in terms of water permeance, we used their characterization results only where needed to support discussions relevant to water permeance. We did not characterize the active layers of ZIF-8-TFNs prepared with calcined ZIF-8 nanofillers (cZIF-8-TFNs) because none of the cZIF-8-TFNs performed better than their corresponding control TFC membranes. As it will become evident in Section 3.2, even though nanofiller incorporation resulted in substantial changes in membrane performance, they were incorporated at relatively low concentrations in the active layers (<1 at.%). Therefore, physico-chemical characterization results for the respective active layers can be assumed to be representative of the polyamide itself with a level of uncertainty within approximately 1 %. A detailed description of the procedures for preparation and analysis of membrane samples for the respective characterization techniques, including active layer isolation from support layers, is provided in Sections A5–A14.

2.7. Evaluation of water permeance and salt rejection

For evaluation of membrane water permeance and NaCl rejection, 8.5 × 11.5 cm^2 membrane coupons were cut from the original 18 × 18 cm^2 membrane sheets. Duplicate coupons were tested for each membrane. The coupons were rinsed with laboratory-grade water and loaded onto a custom-built cross-flow, flat-sheet filtration system with four membrane cells in series (see Fig. A.5 in the Appendix); the active membrane area in each cell was 35.6 cm^2. 0.5 g/L of NaCl solution was supplied to the system as feed. Cross-flow velocity of 16 cm/s, feed temperature of 22 ± 0.2 °C, pH of 6.2 ± 0.3, and applied pressure of 190 psi (for ZIF-8-TFNs) or 200 psi (for LTA-TFNs) were used as test conditions. Water permeance and NaCl rejection data were collected after system performance had stabilized. The reader is referred to the Appendix for additional information on the experimental protocol (Section A15) and equations (Eqs. (A8) and (A9)) for calculation of water permeance and NaCl rejection.

2.8. Statistical analysis

Unless otherwise specified, statistical significance was evaluated using Student's *t*-tests. We used a 90 % confidence level ($p \leq 0.1$) as our metric for assessment of statistical significance. This metric was selected because (i) the purpose of the statistical analysis was to search for evidence of trends, (ii) the number of replicate measurements in membrane studies, including this one, is limited for each condition (*i.e.,* 2–4), and (iii) the solute rejection values of well-performing membranes (>90 % salt rejection) are very close to each other with no more than a few percentage points difference. Whenever statistical comparisons are performed, we provide the *p*-value to enable further interpretation by the reader.

3. Results and discussion

3.1. Membrane performance

3.1.1. Effects of nanofiller loading on membrane performance

Fig. 1(a) summarizes the effects that zeolite loading had on membrane performance in terms of water permeance and NaCl rejection; the corresponding data are summarized in Table A.1 in the Appendix. In general, the results show that the incorporation of nano-zeolites into the respective membrane active layers moderately increased average water permeance without substantially affecting salt rejection up to intermediate nanofiller loadings (0.15–0.30 wt%). However, while further increasing nanofiller loading (0.30–0.75 wt%) continued to increase average water permeance, it also resulted in a substantial decrease in salt rejection. Specifically, nanofiller incorporation up to 0.30 wt% increased average water permeance by 39 % or less and decreased NaCl rejection by ≤0.9 percentage point ($p = 0.573$). This level of change in salt rejection is substantial in full-scale seawater and brackish-water desalination applications, but falls within the uncertainty of membrane casting and testing in bench-scale laboratory settings which, in our experience, is ≤1 percentage point. Further increasing nanofiller loading to 0.75 wt% increased average water permeance by 212 % ($p = 0.004$), but resulted in NaCl rejection plummeting to 72.5 % ($p < 0.001$), rendering the membranes impractical for seawater desalination and most brackish-water desalination applications.

Fig. 1(a) shows enhanced water permeance and comparable contaminant rejection by LTA-TFNs compared to corresponding control TFC membranes. This observation is consistent with results for zeolite TFN membranes reported by others [4,10,35,40–44,137]. For example, a study of NaY zeolite TFN membranes for brackish-water desalination showed that 0.15 wt% nanofiller incorporation increased water permeance by 46 % *versus* the control without substantial decrease in NaCl rejection (98.8 %) [44]. Also, a study on the use of LTA-TFNs in forward osmosis showed enhanced water permeance of TFN membranes *versus* TFC membranes by 79 % at 0.10 wt% zeolite loading, whereas salt rejection decreased to 78 % [43]. Further, in a pilot-scale study of commercially manufactured TFN membranes *versus* TFC membranes, the water permeance was nearly a factor of two higher (47 % higher) for TFN membranes *versus* TFC membranes while presenting generally comparable salt rejection [42]. In a recent study, Salehi et al. prepared TFN membranes using nanostructured zeolite (*i.e.,* clinoptilolite) as nanofillers, and observed permeance enhancement of 43 % and comparable NaCl rejection of 94.7 % (*versus* 96.2 % for TFC membrane) at a nanofiller loading of 0.40 wt% [137].

Fig. 1(b) shows water permeance and percent NaCl rejection for ZIF-8-TFNs as a function of ZIF-8 loading in the TMC organic solution used during active layer casting; the corresponding data are summarized in Table A.2 in the Appendix. The results indicate that average water permeance generally increased as ZIF-8 nanofiller content increased up to a loading of 0.15 wt%, without causing a deleterious impact on NaCl

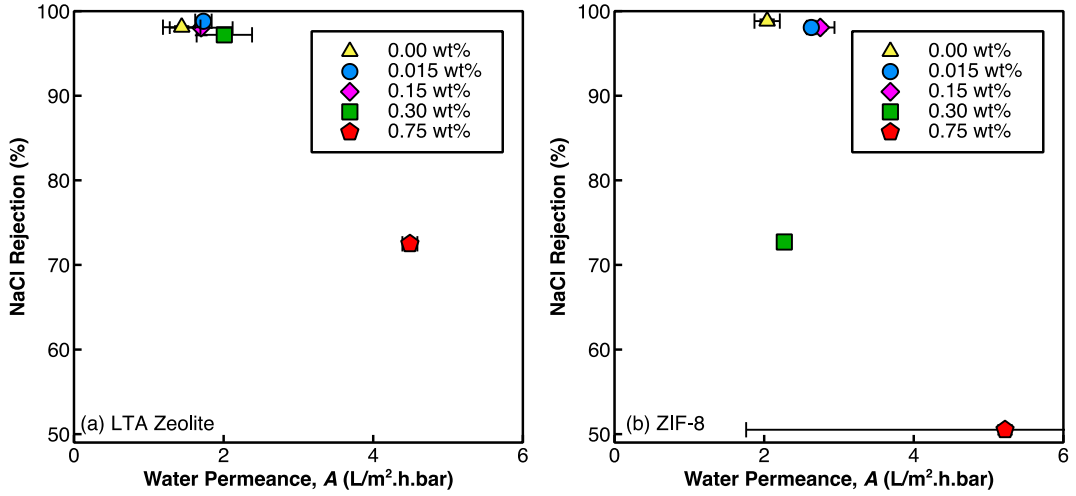

Fig. 1. Percent NaCl rejection (%*R*) *versus* water permeance (*A*) for TFC and TFN membranes with a range of nanofiller loadings. TFC membranes correspond to membranes without nanofillers incorporated (*i.e.,* 0.00 wt%). TFN membranes contained (a) LTA-zeolite and (b) ZIF-8 nanofillers in the active layers. Different batches of chemicals were used in both studies, leading to differences in baseline TFC membrane performance. The legend indicates the percent weight concentration (wt%) of nanofillers in the organic TMC solution during active layer casting. Results reported correspond to the average and standard deviation for duplicate samples. Test conditions: 0.5 g/L NaCl; pH = 6.2 ± 0.3; 190 psi (ZIF-8-TFNs) or 200 psi (LTA-TFNs); and 22 ± 0.2 °C.

rejection performance. Specifically, a 35 % increase in average water permeance was observed at a ZIF-8 loading of 0.15 wt% without significant detrimental effects on NaCl rejection ($p = 0.143$). This trend in water permeance was similar to that observed in the TFN membranes containing LTA-zeolite nanofillers. As shown in Fig. 1(b), while the membranes showed increased average water permeance at ZIF-8 loadings higher than 0.15 wt% (*e.g.,* average 156 % increase *versus* the TFC control at 0.75 wt% ZIF-8 loading), they also demonstrated significant deterioration in salt rejection (*e.g.,* 49 percentage points decrease *versus* the TFC control at 0.75 wt% loading, $p < 0.001$). Others [106,138] have speculated that the reasons why NaCl rejection decreases at higher ZIF-8 loadings are because of the aggregation of nanofillers and formation of defects in the polyamide active layer. The relatively low NaCl rejections exhibited by the TFN membranes with ZIF-8 loadings of 0.30 and 0.75 wt% render them unsuitable for full-scale desalination applications.

The observed trends of increasing water permeance with ZIF-8 loading and drop in salt rejection above a certain ZIF-8 loading threshold were consistent with trends observed in other studies embedding ZIF-8 nanofillers in membrane active layers [69,70,107,108]. For example, Duan et al. evaluated ZIF-8 nanofillers in the selective layer at loadings in the 0.00–0.40 wt% range [70]. At 0.20 and 0.40 wt% loading, Duan and co-workers reported water permeances 124 % and 162 % higher, respectively, than the TFC control without negatively impacting salt rejection performance (>98 %). In another study, Wang et al. prepared ZIF-8-TFNs by incorporating ZIF-8 nanofillers into the aqueous and/or organic phases during active layer casting [108]. TFN membranes with ZIF-8 loadings of 0.15 wt% in either the aqueous or organic phase showed water permeances 46 % and 60 % higher, respectively, than the TFC control. However, the reported salt rejections were 51 % and 38 %, respectively.

When compared to the results for TFN membranes prepared with LTA-zeolite nanofillers, ZIF-8 nanofillers allowed for a greater increase in water permeance without detriment to salt rejection. Specifically, at a nanofiller loading of 0.15 wt%, ZIF-8-TFNs and LTA-TFNs showed a 35 % and 18 % increase, respectively, in water permeance *versus* their corresponding control TFC membranes. Some researchers have hypothesized that the moderately higher water permeance observed in ZIF-8-TFNs *versus* LTA-TFNs may be related to faster water transport through the hydrophobic ZIF-8 structure *versus* the hydrophilic structure in zeolites [68–70].

3.1.2. Effects of nanofiller surface area on membrane performance

To investigate the impacts of nanofiller surface area on TFN membrane performance, we used ZIF-8 nanofillers with a range of surface areas (Fig. 2 and Table A.3). The different surface areas were achieved through calcination (Section 2.3), and the membranes prepared with these nanofillers (0.15 wt%) were labeled as "cZIF-8-TFNs". Corresponding membrane performance results show that incorporation of calcined nanofillers into the active layers had detrimental effects on membrane performance when compared to non-calcined ZIF-8 incorporation. Specifically, compared to the control ZIF-8-TFN, the cZIF-8-TFNs had up to 50 % lower water permeance ($p = 0.017$–0.188) and up to 4.1 percentage points lower salt rejection ($p = 0.006$–0.037). Given that calcined ZIF-8 nanofillers had lower surface areas than their non-calcined counterparts, the results suggest that lower surface areas may lead to decreased water permeance and salt rejection, and thus, that calcination of ZIF-8 nanofillers is not an effective approach to improve performance of ZIF-8-TFNs. Compared to the control TFC, the cZIF-8-TFNs had up to 32 % lower water permeance ($p = 0.060$–0.409) and up to 4.9 percentage points lower salt rejection ($p = 0.001$–0.024).

To the best of the authors' knowledge, there are no existing studies that investigate how calcined ZIF-8 nanofillers influence the structure and performance of membrane active layers. On the other hand, several studies have investigated the influence of calcined MOF materials for absorption and for capture of flue gases [139–142]. For example, Jiang et al. successfully used ZIF-8 nanofillers as template materials to make

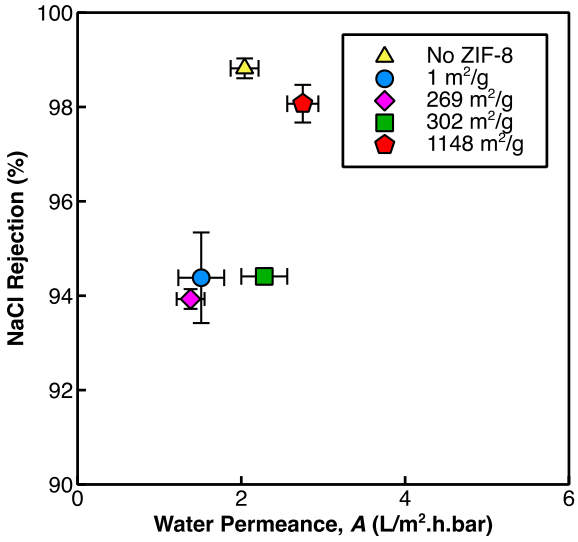

Fig. 2. Percent NaCl rejection (*%R*) *versus* water permeance (*A*) for TFC and TFN membranes prepared with ZIF-8 nanofillers having a range of BET surface areas. TFC membranes correspond to membranes without nanofillers incorporated (*i.e.*, "No ZIF-8"). All TFN membranes in this figure were made using ZIF-8 nanofillers at 0.15 wt% loading in the organic TMC solution used during active layer casting. The non-calcined ZIF-8 surface area was 1148.41 ± 8.29 m^2/g. ZIF-8 surface areas of 301.99 ± 20.27, 268.55 ± 17.52, and 0.96 ± 0.48 m^2/g were obtained using the calcination procedures involving the heating steps at 350, 450, and 550 °C, respectively (see Section A1). Performance results indicate the average and standard deviation for duplicate samples. Test conditions: 0.5 g/L NaCl; pH = 6.2 ± 0.3; 190 psi; and 22 ± 0.2 °C.

nano-porous carbon with exceptionally high BET surfaces areas (~3400 m^2/g) and relatively high hydrogen uptake (2.77 wt% at 77 K and 1 atm) [141]. Srinivas et al. synthesized what they referred to as 'hierarchical porous carbons' from several different MOF materials resulting in carbonized structures displaying surface areas >2000 m^2/g and relatively high CO_2 absorption capabilities (up to 5.53 cm^3/g) [142]. Therefore, it may be possible to find the right set of calcination conditions that would lead to ZIF-8 nanofillers with increased surface areas (over the 1148 m^2/g provided by non-calcined ZIF-8) amenable to incorporation into membrane active layers; however, the procedures reported in this study to produce calcined nanofillers did not result in nanofillers with surface areas larger than that of non-calcined nanofillers. One potential explanation for this is that the imidazolate linkers (melting point of 89–91 °C) of the ZIF-8 materials were compromised from excessive heat exposure during the calcination process, thereby resulting in materials with diminished surface areas [143].

3.1.3. Effects of nanofiller size on membrane performance

To investigate the impacts of nanofiller size on membrane performance, we used ZIF-8 nanofillers with a range of sizes (Fig. 3 and Table A.4). Differences in ZIF-8 nanofiller size were achieved through distinct modifications to the ZIF-8 fabrication procedures as described in Section 2.3. Differences in ZIF-8 nanofiller size were accompanied by differences in ZIF-8 surface area. The resulting ZIF-8 nanofillers had sizes and BET surfaces areas in the ~20–200 nm and 748–1322 m^2/g range, respectively. Membrane performance results (Fig. 3) show that incorporation of non-calcined ZIF-8 nanofillers into the active layers at a 0.15 wt% loading almost always resulted in a substantial increase in water permeance compared to the corresponding control TFCs ($p = 0.022$–0.154). This finding was consistent with the results reported in Section 3.1.1 for LTA-TFNs. Results also show that when the ZIF-8-TFNs were prepared with nanofillers having a narrow size distribution (*i.e.,* ~30, ~65, ~100, or ~150 nm), salt rejection performance was not compromised ($p = 0.142$–0.968). By contrast, ZIF-8-TFNs prepared with

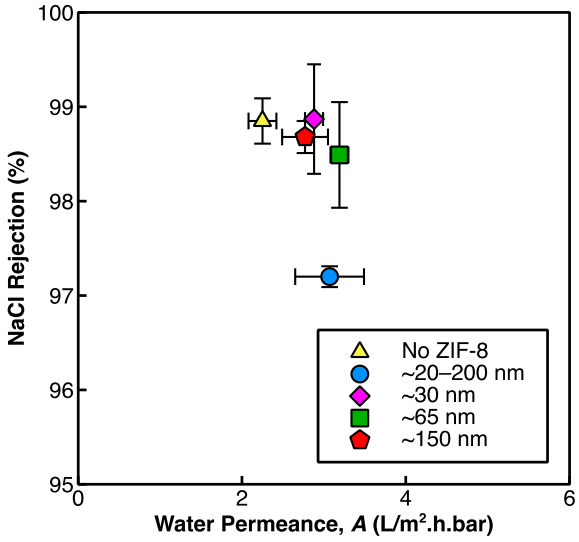

Fig. 3. Percent NaCl rejection (*%R*) *versus* water permeance (*A*) for TFC and TFN membranes prepared with ZIF-8 nanofillers (0.15 wt%) having a range of sizes. TFC membranes correspond to membranes without nanofillers incorporated (*i.e.*, "No ZIF-8"). ZIF-8 nanofiller sizes of ~20–200, ~30, ~65, and ~150 nm were obtained using the ZIF-8 fabrication procedures denoted in Section 2.3 as "no stirring", "double solvent", "15-s stirring", and "titration", respectively; the nanofillers had surface areas of 1275.27 ± 20.48, 795.97 ± 16.53, 1322.20 ± 19.85, and 747.58 ± 9.87 m^2/g, respectively. Results reported indicate the average and standard deviation for quadruplicate samples. Test conditions: 0.5 g/L NaCl; pH = 6.2 ± 0.3; 190 psi; and 22 ± 0.2 °C.

the batch of ZIF-8 nanofillers having a broad distribution of sizes in the ~20–200 nm range had a lower salt rejection than the TFC control (p = 0.013). Therefore, the results indicate that regardless of the ZIF-8 nanofiller size, a 0.15 wt% loading of ZIF-8 nanofillers with a narrow size distribution resulted in increased water permeance without detrimental effects to salt rejection.

Among the ZIF-8-TFNs with similar salt rejections to the control TFC (*i.e.,* those with narrow size distribution), the ones with the highest water permeance increase with respect to their corresponding control TFC were those with ZIF-8 nanofillers of intermediate sizes. Specifically, ZIF-8-TFNs prepared with nanofillers of ~100 nm and ~65 nm in size had water permeances 22 % (p = 0.109) and 42 % (p = 0.022) greater, respectively, than their corresponding control TFCs. The ZIF-8-TFNs with the highest (~150 nm) and smallest (~30 nm) ZIF-8 sizes had water permeances 23 % (p = 0.154) and 28 % (p = 0.048) greater, respectively, than their control TFCs. Thus, it appeared that nanofiller sizes similar in size to active layer thickness (52–92 nm, see Section 3.6) resulted in greater water permeance increases with respect to corresponding control TFCs than ZIF-8 nanofiller sizes significantly different from the active layer thickness.

We also evaluated the performance results of the ZIF-8-TFNs with narrow size distribution from the point of view of their surface areas. The results indicate that the two membranes with the largest water permeance increases, with respect to their corresponding control TFCs, had BET surface areas of 1322.20 ± 19.85 m^2/g (~65 nm ZIF-8 nanofillers) and 1148.41 ± 8.29 m^2/g (~100 nm ZIF-8 nanofillers). The other two membranes had smaller BET surface areas of 747.58 ± 9.87 m^2/g (~150 nm ZIF-8 nanofillers) and 795.97 ± 16.53 m^2/g (~30 nm ZIF-8 nanofillers). Therefore, the results ascertain that larger surface areas correlated with greater increases in water permeance, which was in good agreement with the results for TFN membranes prepared with calcined ZIF-8 nanofillers discussed in Section 3.1.2.

Overall, the results discussed thus far demonstrate that incorporation of nanofillers (*i.e.,* loading) as well as the nanofiller properties (*i.e.,* zeolite *versus* ZIF-8, surface area, and size) play a role in the observed performance differences between TFN membranes and corresponding control TFCs. Therefore, the nanofillers themselves, as well as potentially the polymer-nanofiller interface, play a role in the different performances of TFN membranes and corresponding control TFCs.

3.2. Elemental compositions of membrane active layers

We used LTA-TFNs and ZIF-8-TFNs to evaluate differences in elemental composition between TFN membranes and corresponding TFC controls and the level of nanofiller incorporation into active layers. Table 1 summarizes the elemental compositions of polyamide active layers of LTA-TFNs and corresponding TFC control obtained by X-ray photoelectron spectroscopy (XPS) and Rutherford backscattering spectroscopy (RBS). Elemental content is reported in units of atomic percent (at.%). The RBS elemental compositions reported in Table 1 excluded hydrogen content to allow for easier comparison with XPS results; the corresponding compositions including hydrogen content can be found in Table A.5.

In general, the elemental compositions were similar to those previously reported for commercial RO/NF membranes with polyamide active layers [3,133,144–147]. Elemental compositions were also generally consistent with the range of compositions characteristic of incompletely cross-linked aromatic polyamide, with carbon (C), oxygen (O) and nitrogen (N) contents within the ranges of fully cross-linked aromatic polyamide ($C_{0.75}O_{0.125}N_{0.125}$ excluding hydrogen, or $C_{0.50}O_{0.083}N_{0.083}H_{0.333}$ including hydrogen) and linear aromatic polyamide ($C_{0.714}O_{0.190}N_{0.095}$ excluding hydrogen, or $C_{0.484}O_{0.129}N_{0.065}H_{0.323}$ including hydrogen). For example, C, O, and N contents obtained by XPS were in the 73.10–74.52, 13.53–14.94, and 11.49–12.42 at.% ranges, which were consistent with the theoretical 71.4–75.0, 12.5–19.0, and 9.5–12.5 at.% ranges, respectively. Chlorine (Cl) was found to be present at relatively low concentrations (<0.33 at. %) in the active layers of all membranes tested, consistent with results for commercial membranes used in our previous study [122]. The source of Cl atoms in the polyamide active layer was the acyl chloride moieties in the TMC monomers used during membrane fabrication. No apparent trend in C, O, N, or Cl elemental content was observed as a function of zeolite loading.

As observed in Table 1, aluminum (Al) and silicon (Si), which are the two signature elements of the zeolite nanofillers, were not detected in the respective TFC samples by neither XPS nor RBS. This was consistent with the absence of nanofillers during the TFC casting process. By contrast, while Al and Si were not detected in the LTA-TFNs by RBS, they were detected in small concentrations by XPS. For zeolite loadings up to 0.30 wt%, only Al or Si was detected, and in some cases (0.015 and 0.30 wt%) they were not detected in all locations analyzed over the membrane samples. In contrast, for the highest zeolite loading (0.75 wt%), both Al and Si were detected and at least one of them was detected in each of the four locations analyzed over the membrane samples. The detection of Al and Si in some locations but not in others might be attributed to the combination of relatively low content of zeolites in the active layers (≤0.75 wt% in the TMC casting solution) and relatively small XPS analysis area (300 × 700 μm^2). Nevertheless, the higher consistency of Al and Si detection in the 0.75 wt% LTA-TFN samples suggests that a higher zeolite concentration in the TMC casting solution led to a higher level of zeolite incorporation into the membrane active layer.

In comparing XPS to RBS results, it is important to keep in mind the following two factors: (1) XPS probes the top ~7 nm from the membrane sample surface, whereas RBS provides volume-averaged results for the entire thickness of the active layers; and (2) the total analysis area of RBS was ~2400 mm^2, whereas that of XPS was <1 mm^2. Therefore, RBS results provide a more accurate representation of the overall level of zeolite incorporation in the active layers. Given that neither Al nor Si could be detected through RBS analyses, we conclude that these elements were present at a concentration below the RBS detection limit of

Table 1
Surface (XPS) and bulk-averaged (RBS) properties of TFC (0.00 wt%) and LTA-TFN (0.015, 0.15, 0.30, and 0.75 wt% zeolite loadings) polyamide active layers. Uncertainties represent standard deviation between samples tested. For elemental composition results obtained using RBS, no standard deviations were presented because – for each type of membrane – the RBS spectra of the triplicate samples analyzed were added up and fitted as one single cumulative spectrum to improve accuracy of fitting. The uncertainty of the RBS fitting was <5 %.

Membrane[a]		0.00 wt%	0.015 wt%	0.15 wt%	0.30 wt%	0.75 wt%
C (at.%)	XPS[f]	73.51 ± 0.26	73.55 ± 0.10	73.10 ± 0.25	74.52 ± 1.13	72.16 ± 0.77
	RBS[g]	75.28	76.57	74.70	74.76	74.79
O (at.%)	XPS[f]	13.93 ± 0.59	13.74 ± 0.15	14.82 ± 0.23	13.53 ± 0.50	14.94 ± 0.73
	RBS[g]	12.23	11.56	12.62	12.51	12.52
N (at.%)	XPS[f]	12.26 ± 0.37	12.35 ± 0.21	11.49 ± 0.04	11.61 ± 0.72	12.42 ± 0.90
	RBS[g]	12.23	11.56	12.44	12.51	12.52
Cl (at.%)	XPS[f]	0.29 ± 0.04	0.33 ± 0.05	0.28 ± 0.03	0.26 ± 0.05	0.24 ± 0.09
	RBS[g]	0.25	0.32	0.24	0.23	0.18
Al (at.%)	XPS[f]	0.00 ± 0.00	0.00 ± 0.00	0.32 ± 0.01	0.00 ± 0.00	0.15 ± 0.03
	RBS[g]	BDL[i]	BDL[i]	BDL[i]	BDL[i]	BDL[i]
Si (at.%)	XPS[f]	0.00 ± 0.00	0.03 ± 0.06	0.00 ± 0.00	0.08 ± 0.15	0.08 ± 0.10
	RBS[g]	BDL[i]	BDL[i]	BDL[i]	BDL[i]	BDL[i]
$[R\text{-}COO^-]$[b] (M)	XPS[f]	0.29 ± 0.01	0.34 ± 0.08	0.24 ± 0.02	0.28 ± 0.06	0.35 ± 0.08
	RBS[h]	0.27 ± 0.00	0.23 ± 0.01	0.24 ± 0.03	0.20 ± 0.03	0.17 ± 0.01
$\%\left(\frac{\%R-COO^-}{\%N}\right)$[c]	XPS[f]	2.58 ± 0.14	3.00 ± 0.76	2.31 ± 0.18	2.62 ± 0.42	3.03 ± 1.08
	RBS[h]	2.37 ± 0.00	2.08 ± 0.13	2.08 ± 0.27	1.73 ± 0.24	1.48 ± 0.04
$DPC_{pH=10.5}$[d]	XPS[f]	97.49 ± 0.13	97.09 ± 0.72	97.74 ± 0.17	97.45 ± 0.40	97.06 ± 1.02
	RBS[h]	97.68 ± 0.00	97.96 ± 0.12	97.96 ± 0.26	98.30 ± 0.24	98.55 ± 0.04
n[e]	XPS[f]	0.925 ± 0.004	0.913 ± 0.022	0.932 ± 0.005	0.923 ± 0.012	0.912 ± 0.031
	RBS[h]	0.93 ± 0.000	0.939 ± 0.004	0.939 ± 0.008	0.949 ± 0.007	0.956 ± 0.001
x[e]	XPS[f]	0.075 ± 0.004	0.087 ± 0.022	0.068 ± 0.005	0.077 ± 0.012	0.088 ± 0.031
	RBS[h]	0.070 ± 0.000	0.061 ± 0.004	0.061 ± 0.008	0.051 ± 0.007	0.044 ± 0.001

[a] Indicates weight percent of LTA nano-zeolite in the TMC solution used for active layer casting.
[b] $[R\text{-}COO^-]$: approximated as the molar concentration of silver in Ag^+ probed samples at pH = 10.5.
[c] Average $\%\left(\frac{\%R-COO^-}{\%N}\right)$ values were calculated as the average between the corresponding values for each replicate, not as the ratio between the average %R-COO^- and the average %N.
[d] DPC (degree of polymer cross-linking) ≈ $DPC_{pH=10.5}$ was calculated from Eq. (A5) using the %R-COO^-/%N values at pH = 10.5 shown in the previous row of this table.
[e] n and x represent the fraction of fully aromatic polyamide repeating units that were fully cross-linked ($C_{18}H_{12}N_3O_3$), and that contained a carboxylic group ($C_{15}H_{10}N_2O_4$), respectively, and were calculated assuming that the concentration of amine groups in the active layer was negligible compared to that of carboxylic groups (*i.e.,* $n + x = 1$).
[f] Values in this row correspond to the average of results obtained at 3–5 locations over the same set of three samples analyzed by RBS; there was at least one location analyzed per sample. Elemental content is reported in units of atomic percent.
[g] Values in this row correspond to the cumulative spectrum obtained from three samples totaling an analysis area of ~2400 mm^2 (~800 mm^2 each). Elemental content is reported in units of atomic percent.
[h] Values in this row are the average of three replicates and correspond to the same samples analyzed by XPS.
[i] BDL: below detection limit.

~0.1 at.% for each of Al and Si (see Sections A17 and A18).

Overall, the elemental composition results indicate that zeolite content in the active layers was very small (<1 at.%) and had no substantial effect on the overall elemental composition of the active layer. This suggests that no major changes in the *chemical* structure occurred that could have played a role in the observed changes in membrane performance. For example, the elemental composition of the 0.75 wt% LTA-TFN (*i.e.,* highest zeolite loading, and 3.12 times as much water permeance and 25.6 percentage points lower NaCl rejection than the control TFC) was not substantially different from that of the control TFC, except for the combined presence of Al and Si below 0.23 at.% at the near-surface region.

XPS analysis of the near-surface elemental compositions of ZIF-8-TFNs and corresponding TFC controls (see Table A.6) yielded similar conclusions to those for LTA-TFNs. Specifically, ZIF-8 content in the active layers was also very small (<1 at.%), and had no substantial effect on the overall elemental composition of the active layer. Zinc (Zn) – an element characteristic of ZIF-8 nanofillers – was not detected in the respective TFC samples by XPS. This was consistent with the absence of nanofillers during the TFC casting process. In contrast, Zn was detected in small concentrations in ZIF-8-TFNs at the near-surface region (0.22–0.28 at.%). The elemental compositions of the control TFC and 0.75 wt% ZIF-8-TFN (*i.e.,* highest ZIF-8 loading, and 2.56 times as much water permeance and 48.3 percentage points lower NaCl rejection than the control TFC) were not substantially different, except for the presence of Zn at 0.28 at.% at the near-surface region. These findings were consistent with those of LTA-TFNs in that no major changes in the *chemical* structure occurred that could have played a role in the observed changes in membrane performance.

Additionally, notably, because nanofillers were embedded at such low concentrations in the active layers (<1 at.%), results from physico-chemical characterization tests of the active layer (Sections 3.2–3.7) are representative of the polyamide itself and serve to evaluate whether the polyamide properties differ in TFN membranes compared with control TFCs.

3.3. Degree of polymer cross-linking of membrane active layers

The traditional approach of using the oxygen-to-nitrogen (O:N) ratio to quantify the degree of cross-linking in LTA-TFN membranes could lead to inaccuracies due to the abundance of oxygen in the LTA-zeolite nanofiller and in environmental impurities that may contaminate samples during sample preparation and mounting. Charged sites in the polyamide structure are unreacted acyl chloride groups that hydrolyze into R–COO^- moieties, and therefore each charged site represents a 'broken' link in the polyamide structure [3]. Accordingly, we used the concentrations of charged sites in active layers measured by RBS and XPS analyses to quantify the degree of cross-linking of active layers (Fig. 4 and Table 1). Charged sites are quantified by probing them with silver ion (Ag^+) and quantifying the corresponding silver content in the

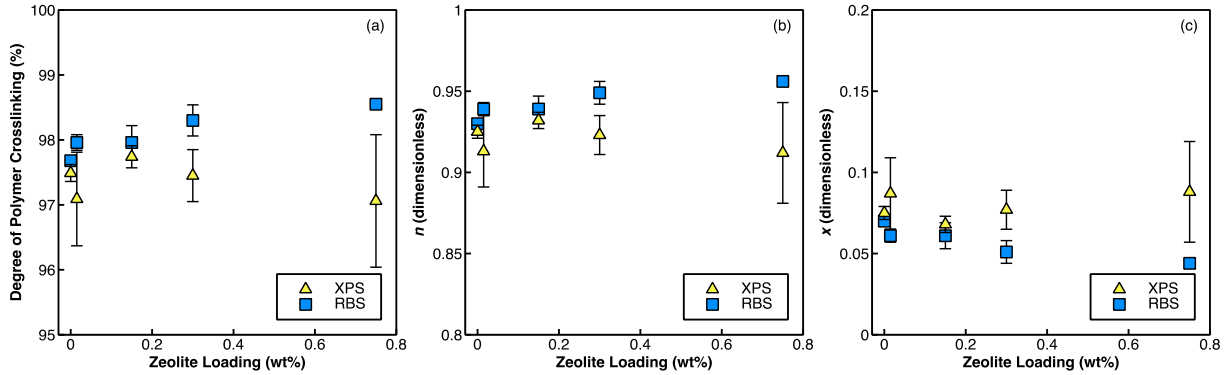

Fig. 4. Degree of cross-linking of membrane active layers measured as (a) degree of polymer cross-linking and as the fractions of polymer repeating units that are (b) fully cross-linked $(C_{0.50}O_{0.083}N_{0.083}H_{0.333})_n$ or (c) contain a broken link in the form of a carboxylic group $(C_{0.484}O_{0.129}N_{0.065}H_{0.323})_x$. XPS and RBS results indicate near-surface and volume-averaged concentrations, respectively. For RBS results, error bars indicate standard deviation for triplicate samples. For XPS results, error bars indicate standard deviation for 3–5 locations over the same set of three samples analyzed by RBS.

membrane sample [133]. This approach improves accuracy in the quantification of degree of cross-linking not just because silver is not present in the original membrane or environmental impurities, but also because both RBS and XPS are substantially more sensitive to silver than to oxygen; more detailed explanations can be found in our previous works [122,133,148]. We used as metrics the degree of polymer cross-linking [133], as well as the fractions of polymer repeating units that are fully cross-linked $(C_{0.50}O_{0.083}N_{0.083}H_{0.333})_n$ or contain a broken link in the form of a carboxylic group $(C_{0.484}O_{0.129}N_{0.065}H_{0.323})_x$ [149].

The results show that the near-surface degree of polymer cross-linking and n fraction of fully cross-linked repeating units were in the 97.06–97.74 % and 0.912–0.932 ranges, respectively, and did not substantially change as a function of zeolite loading. The volume-averaged degree of polymer cross-linking and n fraction were in the 97.68–98.55 % and 0.930–0.956 ranges, respectively, and had a slight increasing trend with increasing zeolite loading, with the highest loading (0.75 wt %) resulting in the highest degree of polymer cross-linking and n fraction. The results therefore indicate that the higher water permeance or decreased salt rejection observed in LTA-TFNs compared to the control TFC was not the result of deterioration in active layer cross-linking.

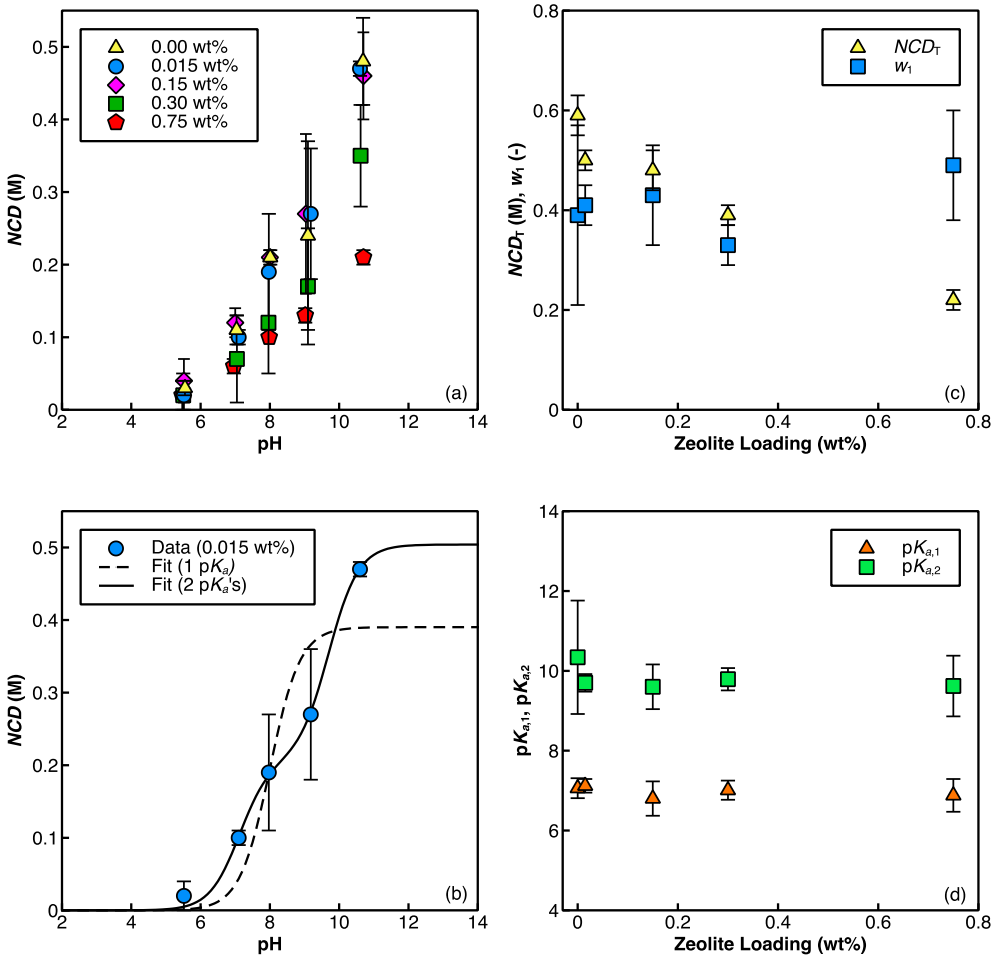

Fig. 5. Ionization behaviors of TFC (0.00 wt %) and LTA-TFN (0.015, 0.15, 0.30, and 0.75 wt% nano-zeolite loading) membrane active layers as a function of pH obtained using active layers isolated on QCM sensors. (a) Experimental data for the concentration of negatively charged sites (NCD) as a function of pH. (b) Representative fit lines of an acid-base model (Eq. (A4) [133]) using unimodal (dashed line, $R^2 = 0.846$) and bimodal (continuous line, $R^2 = 0.999$) pK_a distributions. The data set in panel (b) is that for the TFN membrane with 0.015 wt% nano-zeolite loading; fit lines for the control TFC and the other TFN membranes are presented in Fig. A.7. (c) Values of fitted total concentration of negatively ionizable sites (NCD_T) and fraction of sites with $pK_a = pK_{a,1}$ (w_1). (d) Values of the two fitted acidity constants ($pK_{a,1}$ and $pK_{a,2}$) of the bimodal pK_a distribution describing the ionization behaviors of the active layers. Error bars in (a) and (b) indicate standard deviation of triplicate samples. Error bars in (c) and (d) indicate the uncertainty in the fitting.

A potential source of uncertainty in the calculated degrees of cross-linking is that the zeolites themselves contain charged sites initially in the sodium form; sodium could be exchanged for the silver ions used to probe charged sites and therefore contribute to artificially high charge densities and correspondingly low degrees of cross-linking. As discussed above, the degree of cross-linking of the control TFC was approximately 97.5 % and the degrees of cross-linking of TFN membranes were all similar (97.06–98.55 % including all XPS and RBS results for all membranes, see Table 1). If the observed degrees of cross-linking for TFN membranes were artificially low, then the true degrees of cross-linking would be higher than observed which is not supported by the filtration performance data (*i.e.,* increased nanofiller content led to increased water and salt passage). Further, there is a 1:1 correspondence between the number of charged sites and aluminum atoms in the LTA-zeolite structure ($Na_{12}((AlO_2)_{12}(SiO_2)_{12})\cdot 27H_2O$ [150]) and elemental composition results for TFN membranes (Table 1) indicate aluminum incorporation below 1 at.%. Therefore, any potential artifact in the observed degrees of cross-linking due to nanofiller incorporation is likely relatively low.

3.4. Concentration of charged sites and ionization behaviors of membrane active layers

We evaluated the effects of nanofiller incorporation on the ionization behaviors of membrane active layers as a function of pH (Figs. 5 and 6). The results for LTA-TFNs (Fig. 5) show that the volumetric concentration of charged sites (*NCD*) was always below 0.60 M, which is within the range of values reported in the literature for polyamide active layers [122,123,144,151]. Results also show that *NCD* increased with increasing pH, which is consistent with the ionization behaviors reported previously for active layers of commercial TFC membranes [144,151] and for the TFC and TFN membranes studied in our previous work [123]. The increasing concentration of charged sites with increasing pH is also consistent with the expected deprotonation of carboxylic groups as pH increases [3].

Results show that at all pH values, there was not a substantial difference in *NCD* up to a zeolite loading of 0.15 wt% (Fig. 5(a)). In comparison, a slight or moderate decrease in *NCD* was observed at zeolite loadings of 0.30 and 0.75 wt%, where the latter resulted in the lowest *NCD* values measured. Consistent with this observation, the fitted concentration of volume-averaged charged sites at full ionization (NCD_T) had a moderate decreasing trend with increasing zeolite loading (Fig. 5 (c)). Lower concentrations of charged sites indicate lower active layer hydrophilicity and higher degree of cross-linking (consistent with Fig. 4), each of which would result in lower water permeance as opposed to the increased permeance observed in TFN membranes (Fig. 1(a)) [3,133,149]. Therefore, any potential changes to the concentration of charged sites in the active layer caused by zeolite incorporation did not appear to have played a substantial role in the observed changes in membrane performance.

As illustrated with the 0.015 wt% LTA-TFN in Fig. 5(b), and consistent with results from elsewhere [42,43,123], a unimodal pK_a distribution did not adequately describe the active layer ionization behavior ($R^2 = 0.846$); rather, two pK_a values were required to describe it well ($R^2 = 0.999$). Thus, the data for all membranes were fitted using a bimodal pK_a distribution. Results show that w_1 (and thus w_2), $pK_{a,1}$, and $pK_{a,2}$ did not substantially change with zeolite loading. Therefore, the physico-chemical properties of the active layer that affect ionization of

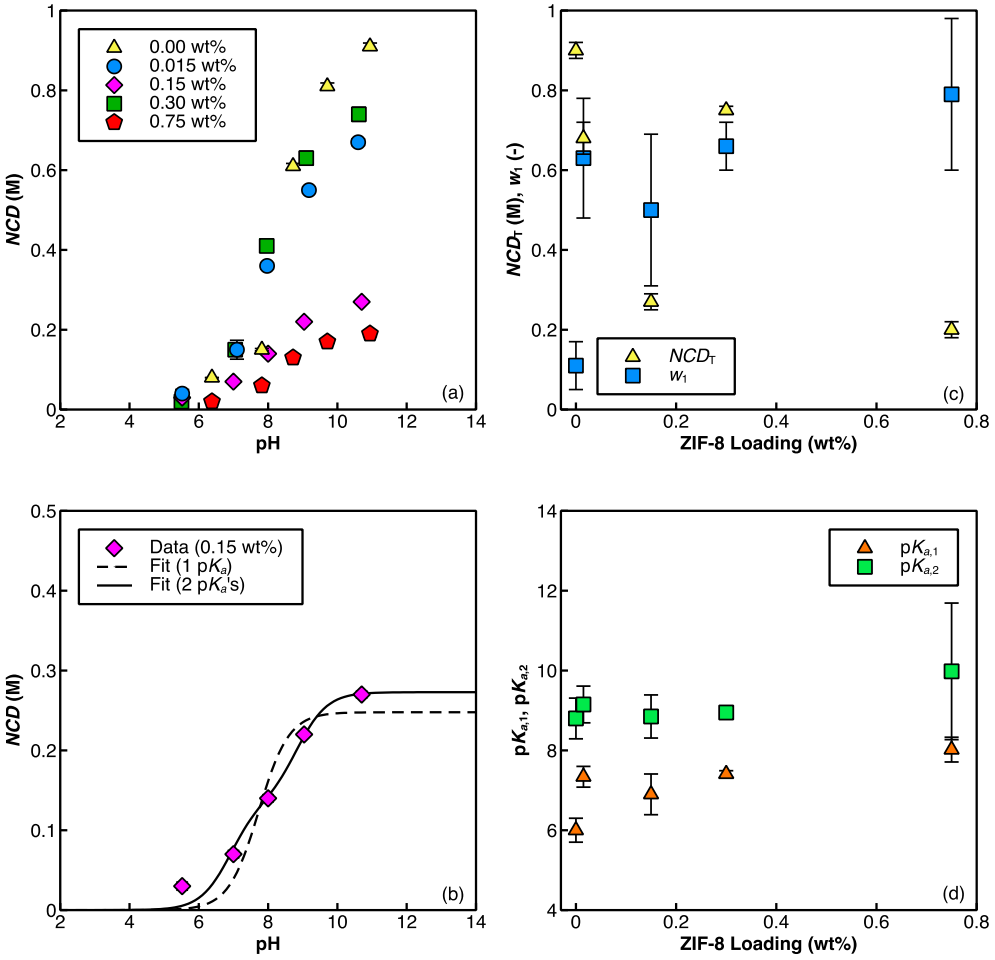

Fig. 6. Ionization behaviors of TFC (0.00 wt %) and ZIF-8-TFN (0.015, 0.15, 0.30, and 0.75 wt% ZIF-8 loading) membrane active layers as a function of pH obtained using active layers isolated on QCM sensors. (a) Experimental data for the concentration of negatively charged sites (*NCD*) as a function of pH. (b) Representative fit lines of acid-base model (Eq. (A4) [133]) using unimodal (dashed line, $R^2 = 0.923$) and bimodal (continuous line, $R^2 = 0.987$) pK_a distributions. The data set in panel (b) is that for the TFN membrane with 0.15 wt% ZIF-8 loading; fit lines for the control TFC and the other TFN membranes are presented in Fig. A.8. (c) Values of fitted total concentration of negatively ionizable sites (NCD_T) and fraction of sites with $pK_a = pK_{a,1}$ (w_1). (d) Values of the two fitted acidity constants ($pK_{a,1}$ and $pK_{a,2}$) of the bimodal pK_a distribution describing the ionization behaviors of the active layers. Error bars in (a) and (b) indicate standard deviation of duplicate samples. Error bars in (c) and (d) indicate the uncertainty in the fitting.

chemical moieties (*e.g.,* dielectric constant, spatial distribution of other chemical moieties) did not substantially change and did not play a substantial role on the observed changes in membrane performance.

Results for the analysis of ionization behaviors of ZIF-8-TFNs with the same ZIF-8 type but different ZIF-8 loadings (Fig. 6) yielded similar conclusions to those for LTA-TFNs (Fig. 5). Specifically, NCD_T results (Fig. 6(c)) indicate that the control TFC had the highest total concentration of charged sites, and that in general a higher ZIF-8 loading - which resulted in a higher water permeance (Fig. 1(b)) - also resulted in a lower total concentration of charged sites. For example, the two ZIF-8-TFNs (0.015 and 0.30 wt%) that had greater water permeance but similar salt rejection to the TFC membrane also had a lower total concentration of charged sites, and thus a higher degree of cross-linking. Therefore, NCD_T results indicate that the observed differences in membrane performance were not related to changes in degree of cross-linking. Also, similar to LTA-TFNs, the ionization behaviors of all ZIF-8-TFNs were best described by a bimodal pK_a distribution (Fig. 6(b)) and neither the values of the acidity constants (*i.e.,* p$K_{a,1}$ and p$K_{a,2}$) nor the relative distribution of sites with p$K_{a,1}$ and p$K_{a,2}$ varied substantially across TFN membranes containing different ZIF-8 loadings (Fig. 6(c)). However, the incorporation of nanofillers did affect membrane ionization behavior, where pK_a's and w_1 were greater for ZIF-8-TFNs than for the control TFC (Fig. 6(c) and (d)). Overall, however, given that different ZIF-8-TFNs had substantially different performances (Fig. 1(b)) but not different ionization behaviors, results indicate that the physicochemical properties of the active layer that affect ionization of chemical moieties did not play a substantial role on the observed changes in membrane performance. It is worth noting that acidity constants (*i.e.,* p$K_{a,1}$ and p$K_{a,2}$) depend on the dielectric constant of the surrounding environment, which in turn is a function of free volume size [133,152–154]. Hence, the minor differences in pK_a values across nanofiller loadings (for both LTA-TFNs and ZIF-8-TFNs) suggest that substantial differences in free volume did not occur.

3.5. Water absorption by membrane active layers

We evaluated the effects of nanofiller incorporation on the absorption of water by active layers of LTA-TFNs and ZIF-8-TFNs when exposed to humidified nitrogen gas at 98 % relative humidity (RH) (Fig. 7). Results for LTA-TFNs (Fig. 7(a)) show that water absorption was in the 0.08–0.15 ng/ng range, consistent with the range of values reported for commercial TFC membranes in previous studies [124,144]. Water sorption showed a slight decreasing trend with increasing zeolite loading. Since the ability of a material to absorb and retain water is largely impacted by its hydrophilicity and secondary forces (*i.e.,* hydrogen bonding), the moderately decreasing trend in water absorption with increasing zeolite loading was consistent with the corresponding moderately decreasing trend in volume-averaged concentration of charged sites described in Section 3.4. Therefore, given that water permeance is directly proportional to water absorption [155], but zeolite incorporation caused a slight decrease in water absorption, then the results indicate that changes in the water absorption properties of the active layers did not substantially contribute to the observed changes in membrane performance.

To study the absorption of water by active layers of ZIF-8-TFNs (Fig. 7(b)), we selected the group of membranes used to study the effects of ZIF-8 nanofiller size on membrane performance (Fig. 3). We selected this group of membranes because these membranes showed significantly different performances from one another only in terms of water permeance. Results show that water absorption was in the 0.05–0.09 ng/ng range, consistent with the low end of the range of values reported for commercial TFC membranes in previous studies [133,141] and LTA-TFN membranes. Water sorption did not show a distinct trend with ZIF-8 nanofiller size, though all average values for ZIF-8-TFNs were slightly lower than that for the control TFC (p = 0.030–0.406). Lower water sorption in ZIF-8-TFNs compared to that in the control TFC might be the result of lower hydrophilicity due to the lower charge density described in Section 3.3. Therefore, given that water permeance is directly proportional to water absorption [133], but ZIF-8 incorporation caused a decrease in water absorption (if any), then the results indicate that changes in the water absorption properties of the active layers did not substantially contribute to the observed changes in membrane performance.

3.6. Thicknesses of membrane active layers

We evaluated the effects of nanofiller incorporation on the active layer thicknesses of LTA-TFNs and ZIF-8-TFNs. Results for the LTA-TFNs (Fig. 8(a)) show that active layer thicknesses were in the 65–109 nm range, with all but the 0.75 wt% LTA-TFN active layer being in the 65–73 nm range. The range of thicknesses obtained was consistent with the range of values reported for commercial TFC membranes in previous studies [125,144]. Active layer thickness did not show an appreciable change with increasing zeolite loading, except at the highest loading (0.75 wt%) at which the thickness (109 nm) was, on average, 57 % higher than for the TFC membrane (69 nm); however, the difference between these two thicknesses was not statistically significant (p = 0.278). Active layer thickness results for ZIF-8-TFNs (Fig. 8(b) and (c))

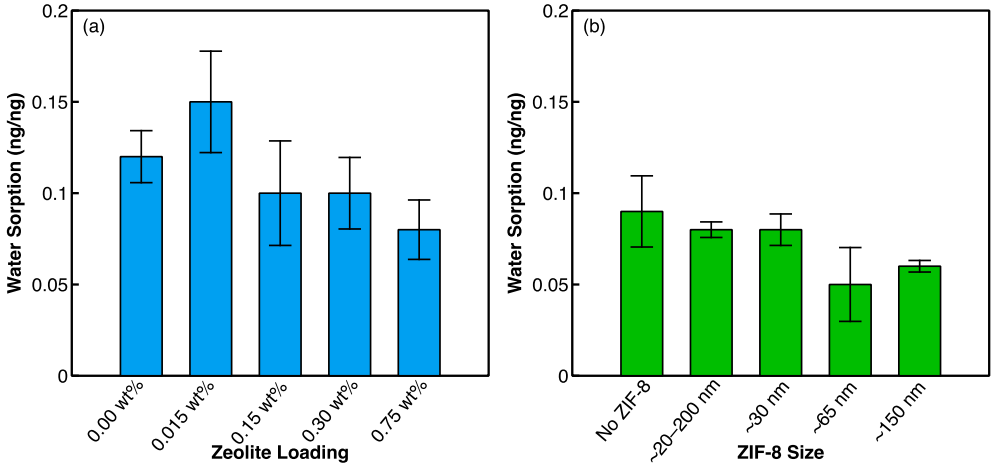

Fig. 7. Water absorption by membrane active layers as a function of (a) zeolite loading and (b) ZIF-8 nanofiller size. Water absorption was measured by exposing active layers isolated on QCM sensors to humidified nitrogen gas at 98 % RH. Results are presented as mass of water absorbed per mass of dry active layer. Data points and error bars indicate average and standard deviation, respectively, of four measurements with two measurements performed in each of duplicate samples.

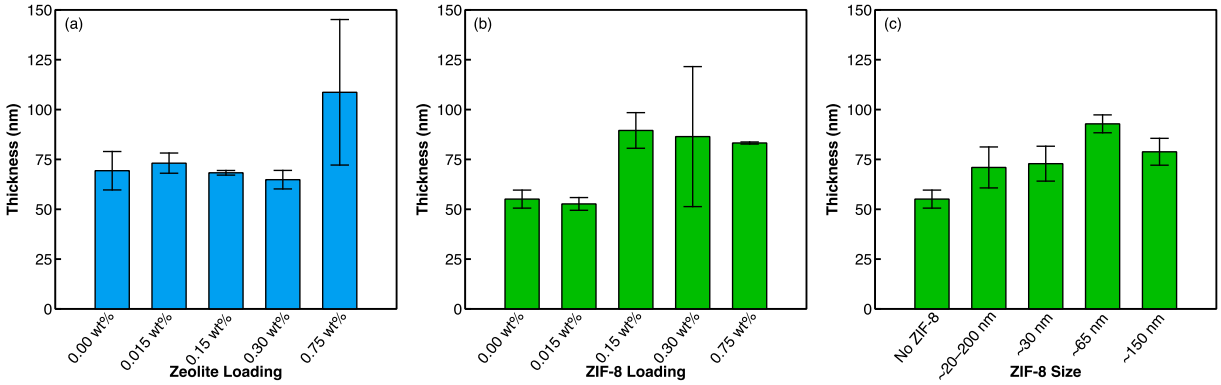

Fig. 8. Active layer thickness as a function of (a) zeolite loading, (b) ZIF-8 loading, and (c) ZIF-8 size. Data points and error bars indicate average and standard deviation, respectively, of duplicate samples.

show that active layer thicknesses were in the 53–92 nm range, which is consistent with the range of thicknesses reported previously for commercial TFC membranes and LTA-TFNs [125,144]. For both the group of ZIF-8-TFNs used to study the effects of ZIF-8 loading (Fig. 8(b)) and the group used to study the effects of ZIF-8 size (Fig. 8(c)), the active layers of all ZIF-8-TFNs had thicknesses that were either similar to or greater than the active layer thickness of the corresponding control TFC.

Since water permeance is inversely dependent on active layer thickness [124], thicker active layers (with all other properties remaining the same) should result in lower water permeances. In contrast, nanofiller incorporation resulted in no change or an increase in active layer thickness accompanied by an increase in water permeance (Figs. 1 and 3). Therefore, the results indicate that the effects of nanofiller incorporation on active layer thickness did not explain the observed changes in membrane performance.

3.7. Surface morphologies of membrane active layers

We evaluated the surface morphologies of TFN membrane active layers *via* quantification of their surface roughness (Fig. 9). This morphological feature was selected for analysis because higher membrane surface roughness has been correlated to higher water permeance, possibly due to increased interfacial area between the membrane surface and the feed solution [156–161]. The results for LTA-TFNs (Fig. 9(a)) show that, in all cases, average surface roughness was in the 59–84 nm range. The range of roughness values obtained was consistent with the range of values reported for commercial TFC membranes in previous studies (~20–150 nm) [122,156–159]. Active layer roughness did not show a specific trend with increasing zeolite loading, and statistical analyses indicate that there was not a significant difference in roughness values between LTA-TFNs and the control TFC (p = 0.472–0.801). Therefore, given that no statistically significant changes were observed on surface roughness with zeolite loadings, the results indicate that any effects that zeolite incorporation had on surface roughness did not play a substantial role on the corresponding observed changes in membrane performance.

The roughness results for ZIF-8-TFNs (Fig. 9(b) and (c)) show that, in all cases, average surface roughness ranged from 22 to 57 nm, which was at the lower end of the range of values obtained for LTA-TFNs (59–84 nm, Fig. 9(a)) and those reported elsewhere for commercially manufactured TFC membranes (~20–150 nm) [156–159]. For the group of ZIF-8-TFNs used to study the effects of ZIF-8 loading (Fig. 9(b)), the only ZIF-8-TFN that had a substantially different roughness from the control TFC was the ZIF-8-TFN with 0.15 wt% ZIF-8 loading (*i.e.*, $p < 0.001$ for 0.15 wt% loading, p = 0.150–0.321 for the remaining ZIF-8 loadings). This correlates well with the higher water permeance of the 0.15 wt% ZIF-8-TFN ($p = 0.060$, see Fig. 1(b)). In contrast, even though the other ZIF-8-TFNs did not have roughness values that were significantly different than the control TFC, these ZIF-8-TFNs had water permeance values very different from the control TFC.

For the group of ZIF-8-TFNs used to study the effects of ZIF-8 size on membrane performance at 0.15 wt% ZIF-8 loading (Fig. 9(c)), all ZIF-8-TFNs had average surface roughness values higher than the control TFC. However, only the roughness values of the ZIF-8-TFNs with the two highest water permeances had significantly greater roughness than the control TFC (p = 0.007–0.046 for the ZIF-8-TFNs with the highest water permeances, p = 0.220–0.552 for the other ZIF-8-TFNs). Specifically, ZIF-8-TFNs with ZIF-8 nanofillers ~65 nm and ~20–200 nm in size had

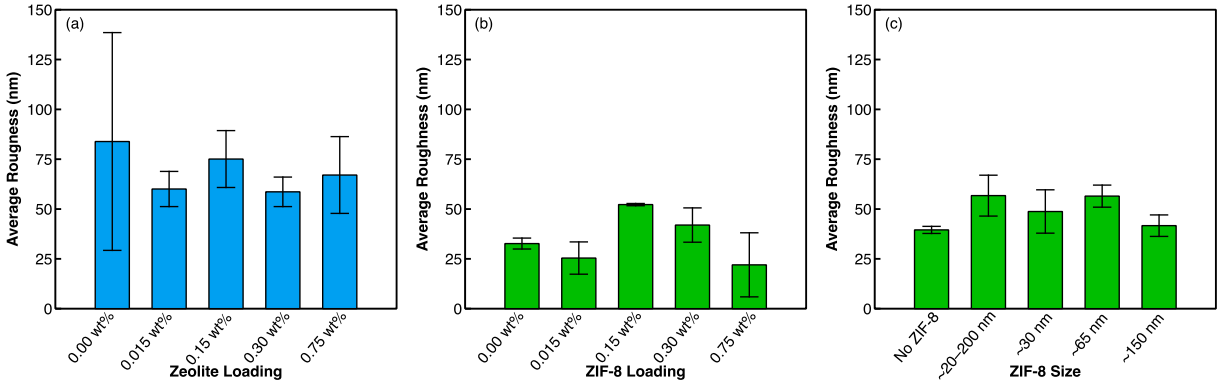

Fig. 9. Membrane surface roughness as a function of (a) zeolite loading, (b) ZIF-8 loading, and (c) ZIF-8 size. Roughness results are presented as average roughness, and were calculated from the atomic force microscopy (AFM) topography data as described elsewhere [126]. Data points and error bars indicate average and standard deviation, respectively, of triplicate samples.

roughness values that were 40–41 % higher than the roughness of the control TFC. In comparison, while the ZIF-8-TFN with ZIF-8 nanofillers ~30 nm in size had a greater average water permeance than the control TFC ($p = 0.048$), its surface roughness was not significantly different than that of the control TFC ($p = 0.220$).

Overall, ZIF-8 incorporation into active layers did not have a consistent effect on surface roughness, and surface roughness results did not have a consistent correlation with water permeance. Therefore, any effects that ZIF-8 incorporation had on surface roughness did not consistently explain the observed changes in membrane performance. This conclusion was consistent with that obtained for zeolite incorporation into active layers.

3.8. Bulk morphologies of membrane active layers

We evaluated the bulk morphologies of the active layers of TFN membranes *via* visualization of their cross-sectional void structures (Fig. 10, Figs. A.9–A.11) as void structure [127,130,162,163] has been reported to impact water permeance [17,24,164–166]. Consistent with the relatively low nanofiller content (<1 at.%) in the TFN active layers (Section 3.2) as well as the corresponding low statistical probability of finding a nanofiller in a random cross-section, no nanofillers were visualized in the transmission-electron-microscopy (TEM) images. The images also show that, consistent with the previously reported presence of voids in the active layers of commercial TFC membranes [127,130,162,163], all active layers had voids in them and no discernable differences in the size or prevalence of voids could be visually observed between the TFN membranes and corresponding TFC controls. Therefore, the TEM images suggest that the incorporation of nanofillers into the membrane active layers did not have an apparent effect on their bulk morphologies and hence did not play a substantial role on the changes observed in membrane performance.

4. Conclusions

A study of properties and performance of TFN membranes embedded with nano-zeolites (LTA-TFNs) and ZIF-8 nanofillers (ZIF-8-TFNs) was conducted to better understand the effects of nanofillers on the physico-chemical properties of the polyamide active layer, and whether the observed effects on physico-chemical properties correlated with observed changes in membrane performance. Results obtained from this study support the following main conclusions:

- At the concentrations that nanofillers were used in casting solutions (*i.e.,* ≤0.15 wt%, typical in the literature and above which salt rejection deteriorates substantially), nanofillers were incorporated into active layers at <1 at.%.
- Because nanofillers were embedded at such low concentrations (*i.e.,* <1 at.%) in the respective active layers, results from physico-chemical characterization tests of TFN active layers are representative of the polymer itself and serve to evaluate whether the polyamide properties differ in TFN membranes compared with control TFCs.
- None of the active layer physico-chemical properties studied in this work trended in a manner that would explain the increased water permeance with increasing nanofiller loading (Table 2).

Because the observed changes in physico-chemical properties of polyamide upon nanofiller incorporation did not account for the observed changes in membrane performance (Table 2), we conclude that

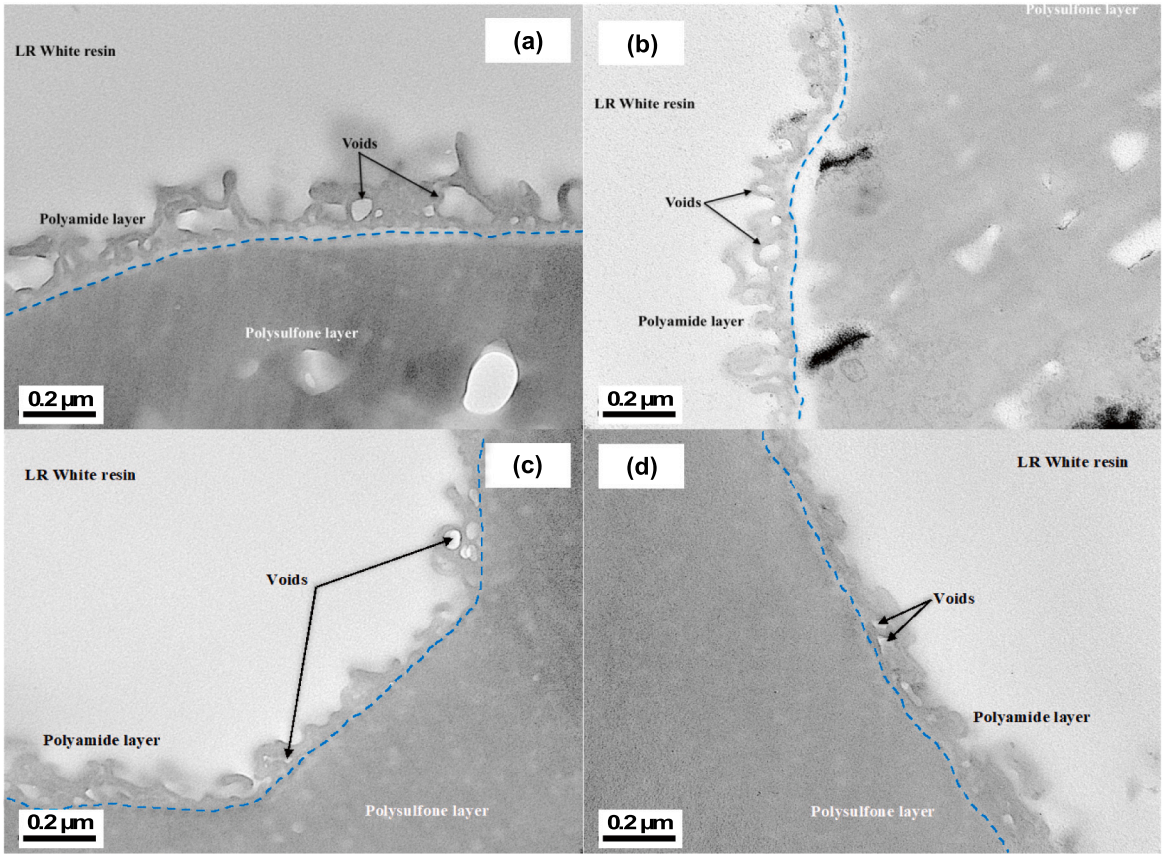

Fig. 10. Representative cross-sectional TEM images of membrane active layers of (a) control TFC prepared for the zeolite study, (b) LTA-TFN with zeolite loading of 0.15 wt%, (c) control TFC prepared for the ZIF-8 study, and (d) ZIF-8-TFN with ZIF-8 loading of 0.15 wt%. Example voids are indicated by arrows. The (blue) dashed line indicates the approximate boundary between the polyamide active layer and the polysulfone support.

Table 2
Trends in change of membrane performance and active layer physico-chemical properties with increasing nanofiller loading.

Property	LTA nano-zeolite	ZIF-8
NaCl rejection	decrease	decrease
Water permeance	increase	increase
DPC	no change or slight increase[a]	not available[b]
NCD	no change or decrease[a]	decrease
Water absorption	decrease	decrease
Thickness	no change[c]	increase
Roughness	no change	no change

[a] Conclusion depends on whether one analyzes RBS or XPS results (Table 1 and Figs. 4 and 5).
[b] We did not measure the DPC of the ZIF-8-TFNs.
[c] The greatest loading (0.75 wt%) had a greater thickness compared with the rest of the LTA-TFNs and TFC.

the increased water permeances of TFN membranes over the control TFCs were primarily the result of water transport through the porous structures of nanofillers or along the polymer-nanofiller interface, as has been suggested to be possible elsewhere [1,4,10,11,34–39,67,114]. Alternatively, properties of the polyamide layer not characterized in this study (*e.g.,* water diffusivity [17]) might have changed, or the topology of the void structure of the selective layer might have been altered in a way that led to greater water permeance but was not quantifiable through the methods used in this study.

CRediT authorship contribution statement

Lamar A. Perry: Conceptualization, Methodology, Validation, Formal analysis, Investigation, Data curation, Writing – original draft, Writing – review & editing, Visualization. **Nick Guan Pin Chew:** Methodology, Validation, Formal analysis, Writing – original draft, Writing – review & editing, Visualization. **Kasia Grzebyk:** Methodology, Writing – review & editing. **Pinar Cay-Durgun:** Methodology, Writing – review & editing. **Mary Laura Lind:** Methodology, Writing – review & editing. **Paban Sitaula:** Methodology, Writing – review & editing. **Mustapha Soukri:** Methodology, Writing – review & editing. **Orlando Coronell:** Conceptualization, Methodology, Writing – review & editing, Formal analysis, Supervision, Funding acquisition.

Declaration of competing interest

The authors declare that they have no known competing financial interests or personal relationships that could have appeared to influence the work reported in this paper.

Data availability

Data will be made available on request.

Acknowledgements

This work was supported by the Dissertation Completion Fellowship (Lamar A. Perry) from the Graduate School of The University of North Carolina at Chapel Hill (UNC-CH). This work was also partially supported by the U.S. National Science Foundation (NSF) (Award Nos. 1264690 and 1336532), National Institute of Environmental Health Sciences (NIEHS) (P42ES031007), and the Water Resources Research Institute (WRRI) of North Carolina and the U.S. Geological Survey (USGS) (WRRI Project #11–03-W, Sub-Award Agreements #2007–01991–11 and 2011–1481–02). RBS analyses were carried out at the Triangle Universities Nuclear Laboratory (TUNL), Durham, NC, which is partially supported by the U.S. Department of Energy (DOE), Office of Science, Office of Nuclear Physics, under Grants DE-FG02-97ER41041 (UNC-CH) and No. DE-FG02-97ER41033 (TUNL). The authors would like to thank Eliot S. Meyer, Dr. Lin Lin, and John Dunham for their assistance in RBS analyses. TEM, SEM, AFM, XPS, and XRD analyses were performed at the Chapel Hill Analytical and Nanofabrication Laboratory (CHANL), a member of the North Carolina Research Triangle Nanotechnology Network (RTNN) which is supported by the National Science Foundation (NSF), Grant #ECCS-2025064, as part of the National Nanotechnology Coordinated Infrastructure (NNCI). The authors would also like to extend their gratitude to Dr. Amar S. Kumbhar for his assistance in the acquisition of TEM, SEM, and AFM images, and Dr. Carrie Donley for her assistance with XPS and XRD analyses.

Appendix A. Supplementary data

Supplementary data to this article can be found online at https://doi.org/10.1016/j.desal.2023.116370.

References

[1] K.P. Lee, T.C. Arnot, D. Mattia, A review of reverse osmosis membrane materials for desalination—Development to date and future potential, J. Membr. Sci. 370 (2011) 1–22.
[2] J.C. Crittenden, D.W. Hand, R.R. Trussell, G. Tchobanoglous, K.J. Howe, Water Treatment: Principles and Design, Third ed., John Wiley & Sons, Incorporated, Hoboken, United States, 2012.
[3] R.J. Petersen, Composite reverse osmosis and nanofiltration membranes, J. Membr. Sci. 83 (1993) 81–150.
[4] M. Duke, D. Zhao, R. Semiat, Functional Nanostructured Materials and Membranes for Water Treatment, Wiley-VCH Verlag GmbH & Co. KGaA, 2013.
[5] M.A. Shannon, P.W. Bohn, M. Elimelech, J.G. Georgiadis, B.J. Mariñas, A. M. Mayes, Science and technology for water purification in the coming decades, Nature 452 (2008) 301–310.
[6] G.M. Geise, H.-S. Lee, D.J. Miller, B.D. Freeman, J.E. McGrath, D.R. Paul, Water purification by membranes: the role of polymer science, J. Polym. Sci. B Polym. Phys. 48 (2010) 1685–1718.
[7] R.H. Hailemariam, Y.C. Woo, M.M. Damtie, B.C. Kim, K.-D. Park, J.-S. Choi, Reverse osmosis membrane fabrication and modification technologies and future trends: a review, Adv. Colloid Interf. Sci. 276 (2020), 102100.
[8] A.W. Mohammad, Y.H. Teow, W.L. Ang, Y.T. Chung, D.L. Oatley-Radcliffe, N. Hilal, Nanofiltration membranes review: recent advances and future prospects, Desalination 356 (2015) 226–254.
[9] M.M. Pendergast, E.M.V. Hoek, A review of water treatment membrane nanotechnologies, Energy Environ. Sci. 4 (2011) 1946–1971.
[10] B.-H. Jeong, E.M.V. Hoek, Y. Yan, A. Subramani, X. Huang, G. Hurwitz, A. K. Ghosh, A. Jawor, Interfacial polymerization of thin film nanocomposites: a new concept for reverse osmosis membranes, J. Membr. Sci. 294 (2007) 1–7.
[11] M. Bassyouni, M.H. Abdel-Aziz, M.S. Zoromba, S.M.S. Abdel-Hamid, E. Drioli, A review of polymeric nanocomposite membranes for water purification, J. Ind. Eng. Chem. 73 (2019) 19–46.
[12] R. Vickers, T.M. Weigand, C.T. Miller, O. Coronell, Molecular methods for assessing the morphology, topology, and performance of polyamide membranes, J. Membr. Sci. 644 (2022), 120110.
[13] A.J. Atkinson, M.D. Armstrong, J.T. Eskew, O. Coronell, 2-aminoimidazole reduces fouling and improves membrane performance, J. Membr. Sci. 629 (2021), 119262.
[14] K. Grzebyk, M.D. Armstrong, O. Coronell, Accessing greater thickness and new morphology features in polyamide active layers of thin-film composite membranes by reducing restrictions in amine monomer supply, J. Membr. Sci. 644 (2022) 120112.
[15] A.J. Atkinson, J. Wang, K. Grzebyk, Z. Zhang, D. Jung, D. Zeng, A. Pollard, A. Gold, O. Coronell, Scalable fabrication of anti-biofouling membranes through 2-aminoimidazole incorporation during polyamide casting, J. Membr. Sci. 579 (2019) 151–161.
[16] A.J. Atkinson, J. Wang, Z. Zhang, A. Gold, D. Jung, D. Zeng, A. Pollard, O. Coronell, Grafting of bioactive 2-aminoimidazole into active layer makes commercial RO/NF membranes anti-biofouling, J. Membr. Sci. 556 (2018) 85–97.
[17] L. Lin, T.M. Weigand, M.W. Farthing, P. Jutaporn, C.T. Miller, O. Coronell, Relative importance of geometrical and intrinsic water transport properties of active layers in the water permeability of polyamide thin-film composite membranes, J. Membr. Sci. 564 (2018) 935–944.
[18] A.C. Fraser, N.G.P. Chew, M. Hegde, F. Liu, C.-W. Liu, O. Coronell, T. J. Dingemans, Linear versus nonlinear aromatic polyamides: the role of backbone geometry in thin film salt exclusion membranes, ACS Appl. Mater. Interfaces 14 (2022) 36143–36156.
[19] V. Freger, G.Z. Ramon, Polyamide desalination membranes: formation, structure, and properties, Prog. Polym. Sci. 122 (2021), 101451.
[20] M. Stolov, O. Keisar, Y. Cohen, V. Freger, Elucidating the effect of aliphatic molecular plugs on ion-rejecting properties of polyamide membranes, ACS Appl. Mater. Interfaces 14 (2022) 13335–13343.

[21] S. Wu, F. Wang, S. Zhou, L. Long, Z. Yang, C.Y. Tang, Vacuum-assisted MPD loading toward promoted nanoscale structure and enhanced water permeance of polyamide RO membrane, Sep. Purif. Technol. 297 (2022), 121547.
[22] S. Zhou, L. Long, Z. Yang, S.L. So, B. Gan, H. Guo, S.-P. Feng, C.Y. Tang, Unveiling the growth of polyamide nanofilms at water/organic free interfaces: toward enhanced water/salt selectivity, Environ. Sci. Technol. 56 (2022) 10279–10288.
[23] Q. Gan, L.E. Peng, H. Guo, Z. Yang, C.Y. Tang, Cosolvent-assisted interfacial polymerization toward regulating the morphology and performance of polyamide reverse osmosis membranes: increased m-phenylenediamine solubility or enhanced interfacial vaporization? Environ. Sci. Technol. 56 (2022) 10308–10316.
[24] L.E. Peng, Y. Jiang, L. Wen, H. Guo, Z. Yang, C.Y. Tang, Does interfacial vaporization of organic solvent affect the structure and separation properties of polyamide RO membranes? J. Membr. Sci. 625 (2021), 119173.
[25] I. Shefer, K. Lopez, A.P. Straub, R. Epsztein, Applying transition-state theory to explore transport and selectivity in salt-rejecting membranes: a critical review, Environ. Sci. Technol. 56 (2022) 7467–7483.
[26] M. Heiranian, R.M. DuChanois, C.L. Ritt, C. Violet, M. Elimelech, Molecular simulations to elucidate transport phenomena in polymeric membranes, Environ. Sci. Technol. 56 (2022) 3313–3323.
[27] J. He, J. Yang, J.R. McCutcheon, Y. Li, Molecular insights into the structure-property relationships of 3D printed polyamide reverse-osmosis membrane for desalination, J. Membr. Sci. 658 (2022), 120731.
[28] X. Chen, R. Verbeke, C. Boo, M. Dickmann, W. Egger, K. Ndamage, I.F. J. Vankelecom, N.Y. Yip, Elucidating the roles of polyamide layer structural properties in the permeability–selectivity tradeoff governing aqueous separations, ACS EST Engg. 2 (2022) 1857–1870.
[29] Z. Yang, H. Guo, C.Y. Tang, The upper bound of thin-film composite (TFC) polyamide membranes for desalination, J. Membr. Sci. 590 (2019), 117297.
[30] G.M. Geise, H.B. Park, A.C. Sagle, B.D. Freeman, J.E. McGrath, Water permeability and water/salt selectivity tradeoff in polymers for desalination, J. Membr. Sci. 369 (2011) 130–138.
[31] H.B. Park, J. Kamcev, L.M. Robeson, M. Elimelech, B.D. Freeman, Maximizing the right stuff: the trade-off between membrane permeability and selectivity, Science 356 (2017), eaab0530.
[32] J.R. Werber, C.O. Osuji, M. Elimelech, Materials for next-generation desalination and water purification membranes, Nat. Rev. Mater. 1 (2016) 16018.
[33] S. Kulprathipanja, R.W. Neuzil, N.N. Li, Separation of fluids by means of mixed matrix membranes, in: US Patent 4,740,219, 1988.
[34] Z. Yang, P.-F. Sun, X. Li, B. Gan, L. Wang, X. Song, H.-D. Park, C.Y. Tang, A critical review on thin-film nanocomposite membranes with interlayered structure: mechanisms, recent developments, and environmental applications, Environ. Sci. Technol. 54 (2020) 15563–15583.
[35] M.L. Lind, B.-H. Jeong, A. Subramani, X. Huang, E.M.V. Hoek, Effect of mobile cation on zeolite-polyamide thin film nanocomposite membranes, J. Mater. Res. 24 (2009) 1624–1631.
[36] Y. Rahimi-Kashkouli, M. Rahbari-Sisakht, A.Ghadami Jadval Ghadam, Thin film nanocomposite nanofiltration membrane incorporated with cellulose nanocrystals with superior anti-organic fouling affinity, Environ. Sci.: Water Res. Technol. 6 (2020) 715–723.
[37] Z.C. Ng, W.J. Lau, T. Matsuura, A.F. Ismail, Thin film nanocomposite RO membranes: review on fabrication techniques and impacts of nanofiller characteristics on membrane properties, Chem. Eng. Res. Des. 165 (2021) 81–105.
[38] D.L. Zhao, S. Japip, Y. Zhang, M. Weber, C. Maletzko, T.-S. Chung, Emerging thin-film nanocomposite (TFN) membranes for reverse osmosis: a review, Water Res. 173 (2020), 115557.
[39] J. Yin, B. Deng, Polymer-matrix nanocomposite membranes for water treatment, J. Membr. Sci. 479 (2015) 256–275.
[40] M.L. Lind, A.K. Ghosh, A. Jawor, X. Huang, W. Hou, Y. Yang, E.M.V. Hoek, Influence of zeolite crystal size on zeolite-polyamide thin film nanocomposite membranes, Langmuir 25 (2009) 10139–10145.
[41] M.L. Lind, D. Eumine Suk, T.-V. Nguyen, E.M.V. Hoek, Tailoring the structure of thin film nanocomposite membranes to achieve seawater RO membrane performance, Environ. Sci. Technol. 44 (2010) 8230–8235.
[42] B. Hofs, R. Schurer, D.J.H. Harmsen, C. Ceccarelli, E.F. Beerendonk, E. R. Cornelissen, Characterization and performance of a commercial thin film nanocomposite seawater reverse osmosis membrane and comparison with a thin film composite, J. Membr. Sci. 446 (2013) 68–78.
[43] N. Ma, J. Wei, R. Liao, C.Y. Tang, Zeolite-polyamide thin film nanocomposite membranes: towards enhanced performance for forward osmosis, J. Membr. Sci. 405–406 (2012) 149–157.
[44] H. Dong, L. Zhao, L. Zhang, H. Chen, C. Gao, W.S. Winston Ho, High-flux reverse osmosis membranes incorporated with NaY zeolite nanoparticles for brackish water desalination, J. Membr. Sci. 476 (2015) 373–383.
[45] J. Yin, E.-S. Kim, J. Yang, B. Deng, Fabrication of a novel thin-film nanocomposite (TFN) membrane containing MCM-41 silica nanoparticles (NPs) for water purification, J. Membr. Sci. 423–424 (2012) 238–246.
[46] M. Kadhom, J. Yin, B. Deng, A thin film nanocomposite membrane with MCM-41 silica nanoparticles for brackish water purification, Membranes 6 (2016) 50.
[47] M. Zargar, Y. Hartanto, B. Jin, S. Dai, Hollow mesoporous silica nanoparticles: a peculiar structure for thin film nanocomposite membranes, J. Membr. Sci. 519 (2016) 1–10.
[48] M.B.M.Y. Ang, J.M. Pereira, C.A. Trilles, R.R. Aquino, S.-H. Huang, K.-R. Lee, J.-Y. Lai, Performance and antifouling behavior of thin-film nanocomposite nanofiltration membranes with embedded silica spheres, Sep. Purif. Technol. 210 (2019) 521–529.
[49] M.B.M.Y. Ang, C.A. Trilles, M.R. De Guzman, J.M. Pereira, R.R. Aquino, S.-H. Huang, C.-C. Hu, K.-R. Lee, J.-Y. Lai, Improved performance of thin-film nanocomposite nanofiltration membranes as induced by embedded polydopamine-coated silica nanoparticles, Sep. Purif. Technol. 224 (2019) 113–120.
[50] Y. Li, C. Li, S. Li, B. Su, L. Han, B. Mandal, Graphene oxide (GO)-interlayered thin-film nanocomposite (TFN) membranes with high solvent resistance for organic solvent nanofiltration (OSN), J. Mater. Chem. A 7 (2019) 13315–13330.
[51] X. Wu, L. Yang, W. Shao, X. Lu, X. Liu, M. Li, Fabrication of high performance TFN membrane incorporated with graphene oxide via support-free interfacial polymerization, Sci. Total Environ. 793 (2021), 148503.
[52] W. Zhao, H. Liu, N. Meng, M. Jian, H. Wang, X. Zhang, Graphene oxide incorporated thin film nanocomposite membrane at low concentration monomers, J. Membr. Sci. 565 (2018) 380–389.
[53] W. Shao, C. Liu, H. Ma, Z. Hong, Q. Xie, Y. Lu, Fabrication of pH-sensitive thin-film nanocomposite nanofiltration membranes with enhanced performance by incorporating amine-functionalized graphene oxide, Appl. Surf. Sci. 487 (2019) 1209–1221.
[54] A. Inurria, P. Cay-Durgun, D. Rice, H. Zhang, D.-K. Seo, M.L. Lind, F. Perreault, Polyamide thin-film nanocomposite membranes with graphene oxide nanosheets: balancing membrane performance and fouling propensity, Desalination 451 (2019) 139–147.
[55] M. Tian, Y.-N. Wang, R. Wang, Synthesis and characterization of novel high-performance thin film nanocomposite (TFN) FO membranes with nanofibrous substrate reinforced by functionalized carbon nanotubes, Desalination 370 (2015) 79–86.
[56] M. Tian, R. Wang, K. Goh, Y. Liao, A.G. Fane, Synthesis and characterization of high-performance novel thin film nanocomposite PRO membranes with tiered nanofiber support reinforced by functionalized carbon nanotubes, J. Membr. Sci. 486 (2015) 151–160.
[57] I. Wan Azelee, P.S. Goh, W.J. Lau, A.F. Ismail, Facile acid treatment of multiwalled carbon nanotube-titania nanotube thin film nanocomposite membrane for reverse osmosis desalination, J. Clean. Prod. 181 (2018) 517–526.
[58] J. Zheng, M. Li, K. Yu, J. Hu, X. Zhang, L. Wang, Sulfonated multiwall carbon nanotubes assisted thin-film nanocomposite membrane with enhanced water flux and anti-fouling property, J. Membr. Sci. 524 (2017) 344–353.
[59] J. Zheng, M. Li, Y. Yao, X. Zhang, L. Wang, Zwitterionic carbon nanotube assisted thin-film nanocomposite membranes with excellent efficiency for separation of mono/divalent ions from brackish water, J. Mater. Chem. A 5 (2017) 13730–13739.
[60] A.O. Rashed, A.M.K. Esawi, A.R. Ramadan, Novel polysulfone/carbon nanotube-polyamide thin film nanocomposite membranes with improved water flux for forward osmosis desalination, ACS Omega 5 (2020) 14427–14436.
[61] Y. Baek, H.J. Kim, S.-H. Kim, J.-C. Lee, J. Yoon, Evaluation of carbon nanotube-polyamide thin-film nanocomposite reverse osmosis membrane: surface properties, performance characteristics and fouling behavior, J. Ind. Eng. Chem. 56 (2017) 327–334.
[62] I. Wan Azelee, P.S. Goh, W.J. Lau, A.F. Ismail, M. Rezaei-DashtArzhandi, K. C. Wong, M.N. Subramaniam, Enhanced desalination of polyamide thin film nanocomposite incorporated with acid treated multiwalled carbon nanotube-titania nanotube hybrid, Desalination 409 (2017) 163–170.
[63] S.R. Mousavi, M. Asghari, N.M. Mahmoodi, Chitosan-wrapped multiwalled carbon nanotube as filler within PEBA thin film nanocomposite (TFN) membrane to improve dye removal, Carbohydr. Polym. 237 (2020), 116128.
[64] V. Dalvi, Y.P. Tang, C. Staudt, T.S. Chung, Influential effects of nanoparticles, solvent and surfactant treatments on thin film nanocomposite (TFN) membranes for seawater desalination, Desalination 420 (2017) 216–225.
[65] A. Tayefeh, S.A. Mousavi, M. Wiesner, R. Poursalehi, Synthesis and surface characterization of magnetite-titania nanoparticles/polyamide nanocomposite smart RO membrane, Procedia Mater. Sci. 11 (2015) 342–346.
[66] N.A. Ahmad, P.S. Goh, A.K. Zulhairun, A.F. Ismail, Antifouling property of oppositely charged titania nanosheet assembled on thin film composite reverse osmosis membrane for highly concentrated oily saline water treatment, Membranes 10 (2020) 237.
[67] T.H. Lee, J.Y. Oh, J.K. Jang, F. Moghadam, J.S. Roh, S.Y. Yoo, Y.J. Kim, T.H. Choi, H. Lin, H.W. Kim, H.B. Park, Elucidating the role of embedded metal–organic frameworks in water and ion transport properties in polymer nanocomposite membranes, Chem. Mater. 32 (2020) 10165–10175.
[68] E.M. Dias, C. Petit, Towards the use of metal–organic frameworks for water reuse: a review of the recent advances in the field of organic pollutants removal and degradation and the next steps in the field, J. Mater. Chem. A 3 (2015) 22484–22506.
[69] Z. Hu, Y. Chen, J. Jiang, Zeolitic imidazolate framework-8 as a reverse osmosis membrane for water desalination: insight from molecular simulation, J. Chem. Phys. 134 (2011), 134705.
[70] J. Duan, Y. Pan, F. Pacheco, E. Litwiller, Z. Lai, I. Pinnau, High-performance polyamide thin-film-nanocomposite reverse osmosis membranes containing hydrophobic zeolitic imidazolate framework-8, J. Membr. Sci. 476 (2015) 303–310.
[71] T.-Y. Liu, H.-G. Yuan, Y.-Y. Liu, D. Ren, Y.-C. Su, X. Wang, Metal–organic framework nanocomposite thin films with interfacial bindings and self-standing robustness for high water flux and enhanced ion selectivity, ACS Nano 12 (2018) 9253–9265.

[72] Y.-Y. Zhao, Y.-L. Liu, X.-M. Wang, X. Huang, Y.F. Xie, Impacts of metal–organic frameworks on structure and performance of polyamide thin-film nanocomposite membranes, ACS Appl. Mater. Interfaces 11 (2019) 13724–13734.
[73] M. He, L. Wang, Y. Lv, X. Wang, J. Zhu, Y. Zhang, T. Liu, Novel polydopamine/metal organic framework thin film nanocomposite forward osmosis membrane for salt rejection and heavy metal removal, Chem. Eng. J. 389 (2020), 124452.
[74] F. Li, T.D. Liu, S. Xie, J. Guan, S. Zhang, 2D metal-organic framework-based thin-film nanocomposite membranes for reverse osmosis and organic solvent nanofiltration, Chem. Sus. Chem. 14 (2021) 2452–2460.
[75] I.H. Aljundi, Desalination characteristics of TFN-RO membrane incorporated with ZIF-8 nanoparticles, Desalination 420 (2017) 12–20.
[76] L. Wang, M. Fang, J. Liu, J. He, J. Li, J. Lei, Layer-by-layer fabrication of high-performance polyamide/ZIF-8 nanocomposite membrane for nanofiltration applications, ACS Appl. Mater. Interfaces 7 (2015) 24082–24093.
[77] M.-P. Li, X. Zhang, H. Zhang, W.-L. Liu, Z.-H. Huang, F. Xie, X.-H. Ma, Z.-L. Xu, Hydrophilic yolk-shell ZIF-8 modified polyamide thin-film nanocomposite membrane with improved permeability and selectivity, Sep. Purif. Technol. 247 (2020), 116990.
[78] X. Wu, L. Yang, F. Meng, W. Shao, X. Liu, M. Li, ZIF-8-incorporated thin-film nanocomposite (TFN) nanofiltration membranes: importance of particle deposition methods on structure and performance, J. Membr. Sci. 632 (2021), 119356.
[79] F. Wang, T. Zheng, R. Xiong, P. Wang, J. Ma, Strong improvement of reverse osmosis polyamide membrane performance by addition of ZIF-8 nanoparticles: effect of particle size and dispersion in selective layer, Chemosphere 233 (2019) 524–531.
[80] T.H. Lee, J.S. Roh, S.Y. Yoo, J.M. Roh, T.H. Choi, H.B. Park, High-performance polyamide thin-film nanocomposite membranes containing ZIF-8/CNT hybrid nanofillers for reverse osmosis desalination, Ind. Eng. Chem. Res. 59 (2020) 5324–5332.
[81] C. Van Goethem, R. Verbeke, M. Pfanmöller, T. Koschine, M. Dickmann, T. Timpel-Lindner, W. Egger, S. Bals, I.F.J. Vankelecom, The role of MOFs in thin-film nanocomposite (TFN) membranes, J. Membr. Sci. 563 (2018) 938–948.
[82] T.H. Lee, J.Y. Oh, S.P. Hong, J.M. Lee, S.M. Roh, S.H. Kim, H.B. Park, ZIF-8 particle size effects on reverse osmosis performance of polyamide thin-film nanocomposite membranes: importance of particle deposition, J. Membr. Sci. 570–571 (2019) 23–33.
[83] A.G. Fane, R. Wang, M.X. Hu, Synthetic membranes for water purification: status and future, Angew. Chem. Int. Ed. 54 (2015) 3368–3386.
[84] C. Wang, X. Liu, J.P. Chen, K. Li, Superior removal of arsenic from water with zirconium metal-organic framework UiO-66, Sci. Rep. 5 (2015) 16613.
[85] Z. Hasan, N.A. Khan, S.H. Jhung, Adsorptive removal of diclofenac sodium from water with zr-based metal–organic frameworks, Chem. Eng. J. 284 (2016) 1406–1413.
[86] H. Furukawa, K.E. Cordova, M. O'Keeffe, O.M. Yaghi, The chemistry and applications of metal-organic frameworks, Science 341 (2013), 1230444.
[87] O.M. Yaghi, M. O'Keeffe, N.W. Ockwig, H.K. Chae, M. Eddaoudi, J. Kim, Reticular synthesis and the design of new materials, Nature 423 (2003) 705–714.
[88] C. Wang, X. Liu, N. Keser Demir, J.P. Chen, K. Li, Applications of water stable metal–organic frameworks, Chem. Soc. Rev. 45 (2016) 5107–5134.
[89] C. Li, S.M. Meckler, Z.P. Smith, J.E. Bachman, L. Maserati, J.R. Long, B.A. Helms, Engineered transport in microporous materials and membranes for clean energy technologies, Adv. Mater. 30 (2018), 1704953.
[90] U. Mueller, M. Schubert, F. Teich, H. Puetter, K. Schierle-Arndt, J. Pastré, Metal–organic frameworks—prospective industrial applications, J. Mater. Chem. 16 (2006) 626–636.
[91] T.A. Makhetha, R.M. Moutloali, Stable zeolitic imidazolate framework-8 supported onto graphene oxide hybrid ultrafiltration membranes with improved fouling resistance and water flux, Chem. Eng. J. Adv. 1 (2020), 100005.
[92] N.A. Ibrahim, M.D.H. Wirzal, N.A.H. Nordin, N.S. Abd Halim, Development of polyvinylidene fluoride (PVDF)-ZIF-8 membrane for wastewater treatment, IOP Conf. Ser.: Earth Environ. Sci. 140 (2018), 012021.
[93] K. Li, N. Miwornunyuie, L. Chen, H. Jingyu, P.S. Amaniampong, D. Ato Koomson, D. Ewusi-Mensah, W. Xue, G. Li, H. Lu, Sustainable application of ZIF-8 for heavy-metal removal in aqueous solutions, Sustainability 13 (2021) 984.
[94] Q. Gu, T.C.Albert Ng, Q. Sun, A.M.Kotb Elshahawy, Z. Lyu, Z. He, L. Zhang, H. Y. Ng, K. Zeng, J. Wang, Heterogeneous ZIF-L membranes with improved hydrophilicity and anti-bacterial adhesion for potential application in water treatment, RSC Adv. 9 (2019) 1591–1601.
[95] K.M. Gupta, K. Zhang, J. Jiang, Water desalination through zeolitic imidazolate framework membranes: significant role of functional groups, Langmuir 31 (2015) 13230–13237.
[96] Y. Wang, W. Zhao, Z. Qi, L. Zhang, Y. Peng, Phosphate removal by ZIF-8@MWCNT hybrids in presence of effluent organic matter: adsorbent structure, wastewater quality, and DFT analysis, Sci. Total Environ. 745 (2020), 141054.
[97] A. Xie, J. Cui, J. Yang, Y. Chen, J. Lang, C. Li, Y. Yan, J. Dai, Dual superlyophobic zeolitic imidazolate framework-8 modified membrane for controllable oil/water emulsion separation, Sep. Purif. Technol. 236 (2020), 116273.
[98] A. Phan, C.J. Doonan, F.J. Uribe-Romo, C.B. Knobler, M. O'Keeffe, O.M. Yaghi, Synthesis, structure, and carbon dioxide capture properties of zeolitic imidazolate frameworks, Acc. Chem. Res. 43 (2010) 58–67.
[99] Y. Pan, Y. Liu, G. Zeng, L. Zhao, Z. Lai, Rapid synthesis of zeolitic imidazolate framework-8 (ZIF-8) nanocrystals in an aqueous system, Chem. Commun. 47 (2011) 2071–2073.
[100] D.W. Breck, Zeolite Molecular Sieves: Structure, Chemistry, and Use, John Wiley & Sons, 1973.
[101] S. Turgman-Cohen, J.C. Araque, E.M.V. Hoek, F.A. Escobedo, Molecular dynamics of equilibrium and pressure-driven transport properties of water through LTA-type zeolites, Langmuir 29 (2013) 12389–12399.
[102] D.W. Breck, W.G. Eversole, R.M. Milton, T.B. Reed, T.L. Thomas, Crystalline zeolites. I. The properties of a new synthetic zeolite, type A 78 (1956) 5963–5972.
[103] C. Baerlocher L.B. McCusker, Database of Zeolite Structures: Framework Type LTA, in.
[104] K.M. Gupta, Z. Qiao, K. Zhang, J. Jiang, Seawater pervaporation through zeolitic imidazolate framework membranes: atomistic simulation study, ACS Appl. Mater. Interfaces 8 (2016) 13392–13399.
[105] Y. Zhu, K.M. Gupta, Q. Liu, J. Jiang, J. Caro, A. Huang, Synthesis and seawater desalination of molecular sieving zeolitic imidazolate framework membranes, Desalination 385 (2016) 75–82.
[106] W. Zhang, Z. Li, Y. Xu, H. Lin, L. Shen, R. Li, M. Zhang, In situ conversion of ZnO into zeolitic imidazolate framework-8 in polyamide layers for well-structured high-permeance thin-film nanocomposite nanofiltration membranes, J. Mater. Chem. A 9 (2021) 7684–7691.
[107] Q. Zhao, D.L. Zhao, T.-S. Chung, Thin-film nanocomposite membranes incorporated with defective ZIF-8 nanoparticles for brackish water and seawater desalination, J. Membr. Sci. 625 (2021), 119158.
[108] L. Wang, M. Fang, J. Liu, J. He, L. Deng, J. Li, J. Lei, The influence of dispersed phases on polyamide/ZIF-8 nanofiltration membranes for dye removal from water, RSC Adv. 5 (2015) 50942–50954.
[109] R. Dai, H. Guo, C.Y. Tang, M. Chen, J. Li, Z. Wang, Hydrophilic selective nanochannels created by metal organic frameworks in nanofiltration membranes enhance rejection of hydrophobic endocrine-disrupting compounds, Environ. Sci. Technol. 53 (2019) 13776–13783.
[110] L. Bai, Y. Liu, N. Bossa, A. Ding, N. Ren, G. Li, H. Liang, M.R. Wiesner, Incorporation of cellulose nanocrystals (CNCs) into the polyamide layer of thin-film composite (TFC) nanofiltration membranes for enhanced separation performance and antifouling properties, Environ. Sci. Technol. 52 (2018) 11178–11187.
[111] L. Valentino, M. Matsumoto, W.R. Dichtel, B.J. Mariñas, Development and performance characterization of a polyimine covalent organic framework thin-film composite nanofiltration membrane, Environ. Sci. Technol. 51 (2017) 14352–14359.
[112] A. Rahimpour, S.F. Seyedpour, S. Aghapour Aktij, M. Dadashi Firouzjaei, A. Zirehpour, A. Arabi Shamsabadi, S. Khoshhal Salestan, M. Jabbari, M. Soroush, Simultaneous improvement of antimicrobial, antifouling, and transport properties of forward osmosis membranes with immobilized highly-compatible polyrhodanine nanoparticles, Environ. Sci. Technol. 52 (2018) 5246–5258.
[113] J. Yin, Z. Yang, C.Y. Tang, B. Deng, Probing the contributions of interior and exterior channels of nanofillers toward the enhanced separation performance of a thin-film nanocomposite reverse osmosis membrane, Environ. Sci. Technol. Lett. 7 (2020) 766–772.
[114] P. Cay-Durgun, S.G. Fink, A. Shabilla, H. Yin, K.A. Sasaki, M.L. Lind, Analysis of the water permeability of linde type a zeolites in reverse osmosis, Sep. Sci. Technol. 49 (2014) 2824–2833.
[115] Z. Yang, H. Guo, Z.-K. Yao, Y. Mei, C.Y. Tang, Hydrophilic silver nanoparticles induce selective nanochannels in thin film nanocomposite polyamide membranes, Environ. Sci. Technol. 53 (2019) 5301–5308.
[116] R. Pang, K. Zhang, Fabrication of hydrophobic fluorinated silica-polyamide thin film nanocomposite reverse osmosis membranes with dramatically improved salt rejection, J. Colloid Interface Sci. 510 (2018) 127–132.
[117] Z. Yang, X. Huang, X.-H. Ma, Z.-W. Zhou, H. Guo, Z. Yao, S.-P. Feng, C.Y. Tang, Fabrication of a novel and green thin-film composite membrane containing nanovoids for water purification, J. Membr. Sci. 570–571 (2019) 314–321.
[118] Z. Yang, J. Yin, B. Deng, Enhancing water flux of thin-film nanocomposite (TFN) membrane by incorporation of bimodal silica nanoparticles, AIMS Environ. Sci. 3 (2016) 185–198.
[119] W.J. Lau, S. Gray, T. Matsuura, D. Emadzadeh, J. Paul Chen, A.F. Ismail, A review on polyamide thin film nanocomposite (TFN) membranes: history, applications, challenges and approaches, Water Res. 80 (2015) 306–324.
[120] P. Cay-Durgun, M.L. Lind, Nanoporous materials in polymeric membranes for desalination, Curr. Opin. Chem. Eng. 20 (2018) 19–27.
[121] J. Li, Y.-N. Wu, Z. Li, B. Zhang, M. Zhu, X. Hu, Y. Zhang, F. Li, Zeolitic imidazolate framework-8 with high efficiency in trace arsenate adsorption and removal from water, J. Phys. Chem. C 118 (2014) 27382–27387.
[122] O. Coronell, B.J. Mariñas, D.G. Cahill, Depth heterogeneity of fully aromatic polyamide active layers in reverse osmosis and nanofiltration membranes, Environ. Sci. Technol. 45 (2011) 4513–4520.
[123] L.A. Perry, O. Coronell, Reliable, bench-top measurements of charge density in the active layers of thin-film composite and nanocomposite membranes using quartz crystal microbalance technology, J. Membr. Sci. 429 (2013) 23–33.
[124] X. Zhang, D.G. Cahill, O. Coronell, B.J. Mariñas, Absorption of water in the active layer of reverse osmosis membranes, J. Membr. Sci. 331 (2009) 143–151.
[125] L. Lin, C. Feng, R. Lopez, O. Coronell, Identifying facile and accurate methods to measure the thickness of the active layers of thin-film composite membranes - a comparison of seven characterization techniques, J. Membr. Sci. 498 (2016) 167–179.
[126] S.-Y. Kwak, S.G. Jung, Y.S. Yoon, D.W. Ihm, Details of surface features in aromatic polyamide reverse osmosis membranes characterized by scanning electron and atomic force microscopy, J. Polym. Sci. B Polym. Phys. 37 (1999) 1429–1440.
[127] L. Lin, R. Lopez, G.Z. Ramon, O. Coronell, Investigating the void structure of the polyamide active layers of thin-film composite membranes, J. Membr. Sci. 497 (2016) 365–376.

[128] H.L. Jamieson, H. Yin, A. Waller, A. Khosravi, M.L. Lind, Impact of acids on the structure and composition of linde type a zeolites for use in reverse osmosis membranes for recovery of urine-containing wastewaters, Microporous Mesoporous Mater. 201 (2015) 50–60.
[129] J. Wang, M.D. Armstrong, K. Grzebyk, R. Vickers, O. Coronell, Effect of feed water pH on the partitioning of alkali metal salts from aqueous phase into the polyamide active layers of reverse osmosis membranes, Environ. Sci. Technol. 55 (2021) 3250–3259.
[130] H. Yan, X. Miao, J. Xu, G. Pan, Y. Zhang, Y. Shi, M. Guo, Y. Liu, The porous structure of the fully-aromatic polyamide film in reverse osmosis membranes, J. Membr. Sci. 475 (2015) 504–510.
[131] J. Xu, H. Yan, Y. Zhang, G. Pan, Y. Liu, The morphology of fully-aromatic polyamide separation layer and its relationship with separation performance of TFC membranes, J. Membr. Sci. 541 (2017) 174–188.
[132] A.K. Ghosh, B.-H. Jeong, X. Huang, E.M.V. Hoek, Impacts of reaction and curing conditions on polyamide composite reverse osmosis membrane properties, J. Membr. Sci. 311 (2008) 34–45.
[133] O. Coronell, B.J. Mariñas, X. Zhang, D.G. Cahill, Quantification of functional groups and modeling of their ionization behavior in the active layer of FT30 reverse osmosis membrane, Environ. Sci. Technol. 42 (2008) 5260–5266.
[134] J. Wang, R.S. Kingsbury, L.A. Perry, O. Coronell, Partitioning of alkali metal salts and boric acid from aqueous phase into the polyamide active layers of reverse osmosis membranes, Environ. Sci. Technol. 51 (2017) 2295–2303.
[135] P.J. Attayek, E.S. Meyer, L. Lin, G.C. Rich, T.B. Clegg, O. Coronell, A remotely controlled, semi-automatic target system for Rutherford backscattering spectrometry and elastic recoil detection analyses of polymeric membrane samples, Nucl. Instrum. Methods Phys. Res. A 676 (2012) 21–25.
[136] J. Powell, J. Luh, O. Coronell, Bulk chlorine uptake by polyamide active layers of thin-film composite membranes upon exposure to free chlorine—Kinetics, mechanisms, and modeling, Environ. Sci. Technol. 48 (2014) 2741–2749.
[137] T.M. Salehi, M. Peyravi, M. Jahanshahi, W.-J. Lau, A.S. Rad, Impacts of zeolite nanoparticles on substrate properties of thin film nanocomposite membranes for engineered osmosis, J. Nanopart. Res. 20 (2018) 113.
[138] Y. Li, J. Li, R.B. Soria, A. Volodine, B. Van der Bruggen, Aramid nanofiber and modified ZIF-8 constructed porous nanocomposite membrane for organic solvent nanofiltration, J. Membr. Sci. 603 (2020), 118002.
[139] N.L. Torad, M. Hu, Y. Kamachi, K. Takai, M. Imura, M. Naito, Y. Yamauchi, Facile synthesis of nanoporous carbons with controlled particle sizes by direct carbonization of monodispersed ZIF-8 crystals, Chem. Commun. 49 (2013) 2521–2523.
[140] M. Majumder, P. Sheath, J.I. Mardel, T.G. Harvey, A.W. Thornton, A. Gonzago, D. F. Kennedy, I. Madsen, J.W. Taylor, D.R. Turner, M.R. Hill, Aqueous molecular sieving and strong gas adsorption in highly porous MOFs with a facile synthesis, Chem. Mater. 24 (2012) 4647–4652.
[141] H.-L. Jiang, B. Liu, Y.-Q. Lan, K. Kuratani, T. Akita, H. Shioyama, F. Zong, Q. Xu, From metal–organic framework to nanoporous carbon: toward a very high surface area and hydrogen uptake, J. Am. Chem. Soc. 133 (2011) 11854–11857.
[142] G. Srinivas, V. Krungleviciute, Z.-X. Guo, T. Yildirim, Exceptional CO2 capture in a hierarchically porous carbon with simultaneous high surface area and pore volume, Energy Environ. Sci. 7 (2014) 335–342.
[143] J.B. James, Y.S. Lin, Kinetics of ZIF-8 thermal decomposition in inert, oxidizing, and reducing environments, J. Phys. Chem. C 120 (2016) 14015–14026.
[144] O. Coronell, M.I. González, B.J. Mariñas, D.G. Cahill, Ionization behavior, stoichiometry of association, and accessibility of functional groups in the active layers of reverse osmosis and nanofiltration membranes, Environ. Sci. Technol. 44 (2010) 6808–6814.
[145] B. Mi, O. Coronell, B.J. Mariñas, F. Watanabe, D.G. Cahill, I. Petrov, Physico-chemical characterization of NF/RO membrane active layers by Rutherford backscattering spectrometry, J. Membr. Sci. 282 (2006) 71–81.
[146] C.Y. Tang, Y.-N. Kwon, J.O. Leckie, Effect of membrane chemistry and coating layer on physiochemical properties of thin film composite polyamide RO and NF membranes: I. FTIR and XPS characterization of polyamide and coating layer chemistry, Desalination 242 (2009) 149–167.
[147] C.Y. Tang, Y.-N. Kwon, J.O. Leckie, Probing the nano- and micro-scales of reverse osmosis membranes—A comprehensive characterization of physiochemical properties of uncoated and coated membranes by XPS, TEM, ATR-FTIR, and streaming potential measurements, J. Membr. Sci. 287 (2007) 146–156.
[148] O. Coronell, M. ter Horst, C. Donley, Microanalysis of reverse osmosis and nanofiltration membranes, in: Encyclopedia of Membrane Science and Technology, 2013, pp. 1–36.
[149] S.H. Kim, S.-Y. Kwak, T. Suzuki, Positron annihilation spectroscopic evidence to demonstrate the flux-enhancement mechanism in morphology-controlled thin-film-composite (TFC) membrane, Environ. Sci. Technol. 39 (2005) 1764–1770.
[150] A. Julbe, M. Drobek, Zeolite A type, in: E. Drioli, L. Giorno (Eds.), Encyclopedia of Membranes, Springer Berlin Heidelberg, Berlin, Heidelberg, 2016, pp. 2055–2056.
[151] A. Tiraferri, M. Elimelech, Direct quantification of negatively charged functional groups on membrane surfaces, J. Membr. Sci. 389 (2012) 499–508.
[152] W.R. Bowen, J.S. Welfoot, Modelling the performance of membrane nanofiltration—critical assessment and model development, Chem. Eng. Sci. 57 (2002) 1121–1137.
[153] A.L. Bacarella, E. Grunwald, H.P. Marshall, E.L. Purlee, The potentiometric measurements of acid dissociation constants and pH in the system methanol-water. pKA values for carboxylic acids and anilinium ions, J. Org. Chem. 20 (1955) 747–762.
[154] S. Senapati, A. Chandra, Dielectric constant of water confined in a nanocavity, J. Phys. Chem. B 105 (2001) 5106–5109.
[155] J.G. Wijmans, R.W. Baker, The solution-diffusion model: a review, J. Membr. Sci. 107 (1995) 1–21.
[156] M. Hirose, H. Ito, Y. Kamiyama, Effect of skin layer surface structures on the flux behaviour of RO membranes, J. Membr. Sci. 121 (1996) 209–215.
[157] S.-Y. Kwak, D. Woo Ihm, Use of atomic force microscopy and solid-state NMR spectroscopy to characterize structure-property-performance correlation in high-flux reverse osmosis (RO) membranes, J. Membr. Sci. 158 (1999) 143–153.
[158] S.S. Madaeni, The effect of surface characteristics on RO membrane performance, Desalination 139 (2001) 371.
[159] S. Al-Jeshi, A. Neville, An investigation into the relationship between flux and roughness on RO membranes using scanning probe microscopy, Desalination 189 (2006) 221–228.
[160] N.G.P. Chew, Y. Zhang, K. Goh, J.S. Ho, R. Xu, R. Wang, Hierarchically structured janus membrane surfaces for enhanced membrane distillation performance, ACS Appl. Mater. Interfaces 11 (2019) 25524–25534.
[161] N.G.P. Chew, S. Zhao, R. Wang, Recent advances in membrane development for treating surfactant- and oil-containing feed streams via membrane distillation, Adv. Colloid Interf. Sci. 273 (2019) 102022.
[162] F. Pacheco, R. Sougrat, M. Reinhard, J.O. Leckie, I. Pinnau, 3D visualization of the internal nanostructure of polyamide thin films in RO membranes, J. Membr. Sci. 501 (2016) 33–44.
[163] M.M. Kłosowski, C.M. McGilvery, Y. Li, P. Abellan, Q. Ramasse, J.T. Cabral, A. G. Livingston, A.E. Porter, Micro-to nano-scale characterisation of polyamide structures of the SW30HR RO membrane using advanced electron microscopy and stain tracers, J. Membr. Sci. 520 (2016) 465–476.
[164] M.C.Y. Wong, L. Lin, O. Coronell, E.M.V. Hoek, G.Z. Ramon, Impact of liquid-filled voids within the active layer on transport through thin-film composite membranes, J. Membr. Sci. 500 (2016) 124–135.
[165] X.-H. Ma, Z.-K. Yao, Z. Yang, H. Guo, Z.-L. Xu, C.Y. Tang, M. Elimelech, Nanofoaming of polyamide desalination membranes to tune permeability and selectivity, Environ. Sci. Technol. Lett. 5 (2018) 123–130.
[166] Y. Wen, X. Zhang, X. Li, Z. Wang, C.Y. Tang, Metal–organic framework nanosheets for thin-film composite membranes with enhanced permeability and selectivity, ACS Appl. Nano Mater. 3 (2020) 9238–9248.